Cell

Resource

A Nanobody-Based System Using Fluorescent Proteins as Scaffolds for Cell-Specific Gene Manipulation

Jonathan C.Y. Tang,[1,2] Tamas Szikra,[4] Yevgenia Kozorovitskiy,[1,3] Miguel Teixiera,[4,5] Bernardo L. Sabatini,[1,3] Botond Roska,[4] and Constance L. Cepko[1,2,*]
[1]Howard Hughes Medical Institute
[2]Departments of Genetics and Ophthalmology
[3]Department of Neurobiology
Harvard Medical School, Boston, MA 02115, USA
[4]Neural Circuit Laboratories, Friedrich Miescher Institute for Biomedical Research, 4058 Basel, Switzerland
[5]University of Basel, 4003 Basel, Switzerland
*Correspondence: cepko@genetics.med.harvard.edu
http://dx.doi.org/10.1016/j.cell.2013.07.021

SUMMARY

Fluorescent proteins are commonly used to label cells across organisms, but the unmodified forms cannot control biological activities. Using GFP-binding proteins derived from Camelid antibodies, we co-opted GFP as a scaffold for inducing formation of biologically active complexes, developing a library of hybrid transcription factors that control gene expression only in the presence of GFP or its derivatives. The modular design allows for variation in key properties such as DNA specificity, transcriptional potency, and drug dependency. Production of GFP controlled cell-specific gene expression and facilitated functional perturbations in the mouse retina and brain. Further, retrofitting existing transgenic GFP mouse and zebrafish lines for GFP-dependent transcription enabled applications such as optogenetic probing of neural circuits. This work establishes GFP as a multifunctional scaffold and opens the door to selective manipulation of diverse GFP-labeled cells across transgenic lines. This approach may also be extended to exploit other intracellular products as cell-specific scaffolds in multicellular organisms.

INTRODUCTION

Studies of multicellular organisms would be greatly facilitated by the ability to manipulate the activities of any genes within specific tissues or cell types. This is challenging to achieve in tissues with diverse cell types, such as the nervous system (Masland, 2004). To label and provide genetic access to diverse cell types, much effort has been devoted to generating transgenic organisms in which transgenes are placed under the control of large genomic fragments or endogenous gene loci. Transgenic lines expressing driver genes such as transcription factors or site-specific recombinases in specific cell populations can then be used to control the expression of genes in responder cassettes. However, the utility of individual lines is limited by a transgene's functional abilities; reporter lines expressing fluorescent proteins and histochemical enzymes are useful for labeling cells but cannot currently be used to control biological activities. To replace transgenes driven by the same *cis*-regulatory elements requires generation of additional transgenic lines. Such a procedure can be costly and lengthy for organisms such as the mouse. Thus, a key to conducting efficient and wide-ranging studies on existing and future model organisms is to increase the versatility of transgenic resources.

Owing to their ease of detection, GFP and its derivatives (Tsien, 1998) have become common markers of gene expression (Chalfie et al., 1994) across model organisms. Notably, thousands of transgenic GFP lines have been generated for the mouse (Gong et al., 2003). This growing and important resource reveals the expression pattern of many genes and provides strains in which GFP selectively labels many cell types of interest (http://www.gensat.org/index.html; Siegert et al., 2009). Transgenic GFP lines have enabled applications such as cell-type-specific transcriptome profiling, as well as targeted anatomical and physiological analysis (Huang et al., 2003; Siegert et al., 2012). However, functional manipulation of GFP-labeled cell types often requires the use of driver lines such as those that express Cre, which currently exist in limited numbers.

A system converting GFP expression into desired molecular outputs would enable existing and future transgenic GFP lines to be used directly for gene manipulation in specific cell types. Synthetic RNA devices have been engineered to convert the presence of an intracellular protein into gene expression output (Culler et al., 2010). Although promising, protein-responsive RNA devices await application in animals (Chang et al., 2012). Meanwhile, artificially derived binding proteins, herein including antibodies and unrelated proteins with ideal structures for evolving target recognition (Wurch et al., 2012), are being used

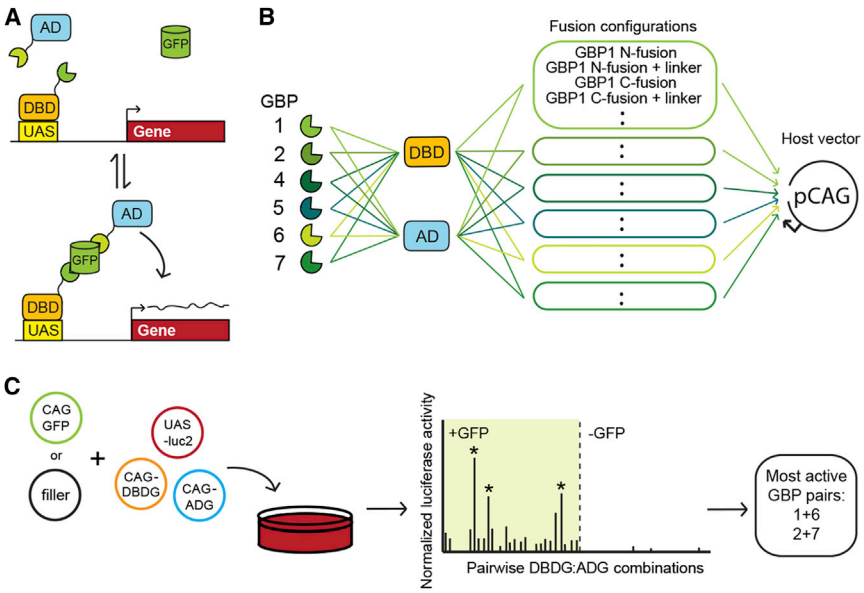

Figure 1. In Vitro Screen Used to Identify Functional GBP Pairs for the GFP-Dependent Transcription System

(A) Schematic of GFP-dependent transcription system. DBD, DNA-binding domain; AD, activation domain; UAS, upstream activating sequence.

(B) Strategy for making DBD-GBP (DBDG) or AD-GBP (ADG) fusion constructs used in the screen for T-DDOGs. All genes were controlled by the CAG promoter in pCAG vector.

(C) Schematic of typical in vitro luciferase screen for functional GBP-fusion combinations capable of inducing GFP-dependent transcription. See also Table S1.

intracellularly to target proteins in cells and organisms. Thus far, these reagents are used for target-centric purposes such as protein interference (Jobling et al., 2003), degradation (Caussinus et al., 2012), and modulation (Kirchhofer et al., 2010). Artificially derived binding proteins could possibly be a powerful platform to co-opt intracellular proteins as cell-specific signals that control synthetic circuits, without modifications to the target protein or reliance on the target protein's natural interactions or functions.

We explored whether artificially derived binding proteins can confer GFP with the ability to regulate genes. GFP seems relatively inert in many heterologous systems; it is freely diffusible in the cytoplasm, can enter the nucleus, confers low cytotoxicity, and has few interactions with host proteins (Trinkle-Mulcahy et al., 2008). The development of GFP-binding proteins (GBPs) from Camelid antibodies (Kirchhofer et al., 2010) has made possible the construction of GBP-fusion proteins noncovalently linking GFP to a variety of proteins in living cells (Caussinus et al., 2012). These reagents, termed nanobodies, are single-chain antigen-binding domains that are relatively small in size (~300–400 bp) and can be easily expressed in living cells (Rothbauer et al., 2006). Given the availability of multiple GBPs, we reasoned that GFP might be used as a scaffold to organize the formation of biologically active complexes. In one scheme, GFP would act like a small-molecule "dimerizer," bridging the association of distinct modular domains or protein fragments to reconstitute useful activities such as transcription and recombination (Jullien et al., 2003; Pollock and Clackson, 2002).

Here, we identified pairs of GBPs that can recruit tethered proteins onto the GFP scaffold, providing the means by which GFP-inducible systems can be built. We developed a GFP-dependent transcription system with these reagents, enabling control of any target gene for functional studies across tissues and organisms. The modular design of the transcription system allowed for straightforward and predictable changes to critical features such as DNA binding specificity, transcriptional potency, and drug dependency. Our work extends the functionality of GFP into the regulatory realm, thus opening the door to selective manipulation of GFP-labeled cells across transgenic GFP lines and establishing components for the design of synthetic circuits.

RESULTS

Design and Isolation of GFP-Dependent Transcription Factors

In order to use GFP as a dimerizer, one has to identify GBP pairs that can bind to GFP at the same time. Suitable GBP pairs could then bring together fusion protein partners on the GFP scaffold. We obtained six GBPs for this purpose (Kirchhofer et al., 2010). Several GBPs were reported to bind additively to a preformed GFP-GBP1 complex when tested as purified proteins in vitro (Kirchhofer et al., 2010). However, it was unclear whether any of the identified pairs could co-occupy GFP, tolerate the addition of fusion partners, and induce the formation of biologically active complexes in cells. Furthermore, many possible GBP pair-wise combinations had not been tested for their ability to co-occupy GFP. To address these issues, we performed an in vitro reporter screen for GBP pairs that could induce the formation of an active transcription factor (Figure 1 and Extended Experimental Procedures). The Gal4 DNA-binding domain (DBD) and VP16 activation domain (AD) (Sadowski et al., 1988) were separately fused to GBPs in various configurations and placed under control of the ubiquitous CMV early enhancer/chicken β actin (CAG) promoter (Niwa et al., 1991) (Figure 1B). DBD-GBP (DBDG) and AD-GBP (ADG) fusion constructs were screened in pair-wise combinations for GFP-dependent activation of an upstream activating sequence-regulated luciferase (UAS-luc2) reporter in 293T cells. Functional DBDG/ADG pairs will be referred to as transcription devices dependent on GFP (T-DDOG). T-DDOGs employing GBP1+6 or GBP2+7 consistently gave the strongest reporter induction (Figures 1C, 2, and S1 available online) and became the focus of this study. To specify DBDG+ADG combinations, the DBD-GBPX fusion is listed in regular font, along with

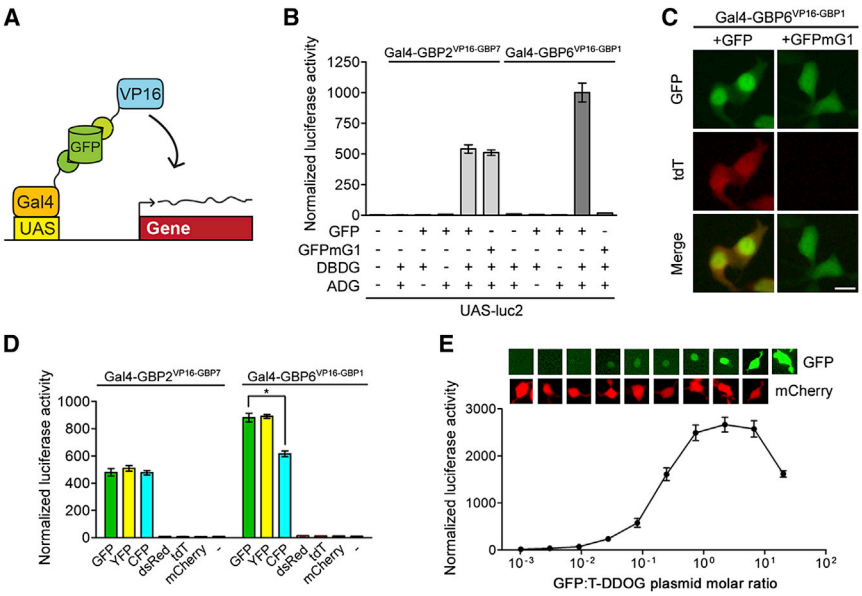

Figure 2. Characterization of the GFP-Dependent Transcription System

(A) Schematic of Gal4-based T-DDOGs.

(B) GFP-dependent activation of UAS-luc2 by Gal4-GBP6$^{VP16\text{-}GBP1}$ and Gal4-GBP2$^{VP16\text{-}GBP7}$. n = 9.

(C) Gal4-GBP6$^{VP16\text{-}GBP1}$ strongly activated UAS-tdT in the presence of GFP. Mutation of GBP1-binding residues in GFP (GFPmG1) abolished tdT activity. Scale bar, 10 μm.

(D) Specificity of T-DDOGs for different fluorescent proteins. n = 9; *p < 0.001.

(E) Activity of Gal4-GBP6$^{VP16\text{-}GBP1}$ in response to a varying amount of transfected GFP plasmids. The transfected DNA amount was kept constant among conditions, with CAG-mCherry (bottom) acting as a filler plasmid to compensate for reduction in GFP (top) plasmids. Panels show representative GFP and mCherry fluorescence in single cells for each corresponding data point below. n = 6. Plots are mean ± SD.

See also Figures S1 and S2 and Table S2.

the AD-GBPX fusion in superscript, giving DBD-GBPX$^{AD\text{-}GBPY}$. Specific T-DDOG configurations are tabulated in Table S1.

Characterization of the GFP-Dependent Transcription System In Vitro

The induced transcription output in 293T cells was found to be dependent on all components of the system, as removal of GFP, DBDG, or ADG from the transfection mixture resulted in loss of reporter activity (Figures 2B and S1). Reporter induction was further dependent on the ability of GBP to bind to GFP. Based on the GBP1 + GFP crystal structure (Kirchhofer et al., 2010), we mutated GFP residues expected to directly interact with GBP1. One such variant, GFPmG1, carries the mutations E143K and N147Q. Like GFP, GFPmG1 was localized to the nucleus by the VP16AD-GBP7 fusion protein (Figure S2). However, unlike GFP, GFPmG1 was not localized to the nucleus by the VP16AD-GBP1 fusion protein (Figure S2). In agreement with this, GFPmG1 induced strong UAS-reporter in the presence of Gal4-GBP2$^{VP16\text{-}GBP7}$, but not Gal4-GBP6$^{VP16\text{-}GBP1}$ (Figures 2B, 2C, and S1 and Table S2). These data confirm a requirement for GFP-GBP interactions and suggest that GBP2 and GBP7 do not depend critically on residue 143 or 147 for binding to GFP.

We also tested whether T-DDOG activity can be controlled by the GFP derivatives cyano and yellow fluorescent proteins (CFP and YFP) and the Discosoma-derived red fluorescent proteins dsRed, mCherry, and tdTomato (tdT) (Shaner et al., 2005). CFP and YFP induced Gal4-GBP2$^{VP16\text{-}GBP7}$ activity to a similar extent as GFP (Figure 2D). However, CFP had reduced ability to activate Gal4-GBP6$^{VP16\text{-}GBP1}$. This was expected because CFP differs from GFP at the GBP1-interacting residue 147 (Rothbauer et al., 2008). Also as expected, none of the red fluorescent proteins could induce T-DDOG activity. In support of this, red fluorescent proteins were diffusely distributed in the cell even when T-DDOG components were clearly localizing GFP to the nucleus (Figures 2C and 2E).

To evaluate the effect of GFP level on T-DDOG activity, we varied the amount of GFP plasmid delivered to 293T cells and examined UAS-luc2 expression in the presence of Gal4-GBP6$^{VP16\text{-}GBP1}$. The observations were consistent with those reported for small-molecule dimerizers (Ho et al., 1996). T-DDOG activity increased linearly with the amount of transfected GFP until a certain point, beyond which further increases in GFP led to reduction of activity. The reduced activity is likely due to titration of T-DDOG components by GFP. Interestingly, GFP was highly enriched in the nucleus at levels correlating with the rising phase of the dosage curve but spread into the cytoplasm at levels correlated with the declining phase of the curve (Figure 2E).

Modularity of GFP-Dependent Transcription System Permits Various Adjustments and Fine-Tuning

Transcription factors are highly modular (Luan et al., 2006; Sadowski et al., 1988). To exploit this feature for creating a diversity of T-DDOGs with varying properties, we substituted the transcription domains in our original GBP fusion library with other commonly used ones and conducted additional in vitro screens. Indeed, we were able expand and diversify the functional repertoire of T-DDOGs. T-DDOGs using the rTetR and LexA DBDs activated reporters bearing their respective binding sequences, tetO (included in tetracycline response element, TRE) and lexAop, only when GFP was present (Figures 3A–3E) (Butala et al., 2009; Schönig et al., 2010). The activities of rTetR-based T-DDOGs were further found to depend on doxycycline levels (Figure 3D). This drug dependency provides temporal control for the system.

T-DDOGs can also be adjusted to alter their transcriptional potency. The critical region for VP16AD function lies within a 12 amino acid peptide (VPmin) (Baron et al., 1997). We could predictably adjust the transcriptional activity of Gal4-GBP1$^{AD\text{-}GBP6}$ by either varying the number of VPmin repeats or the number

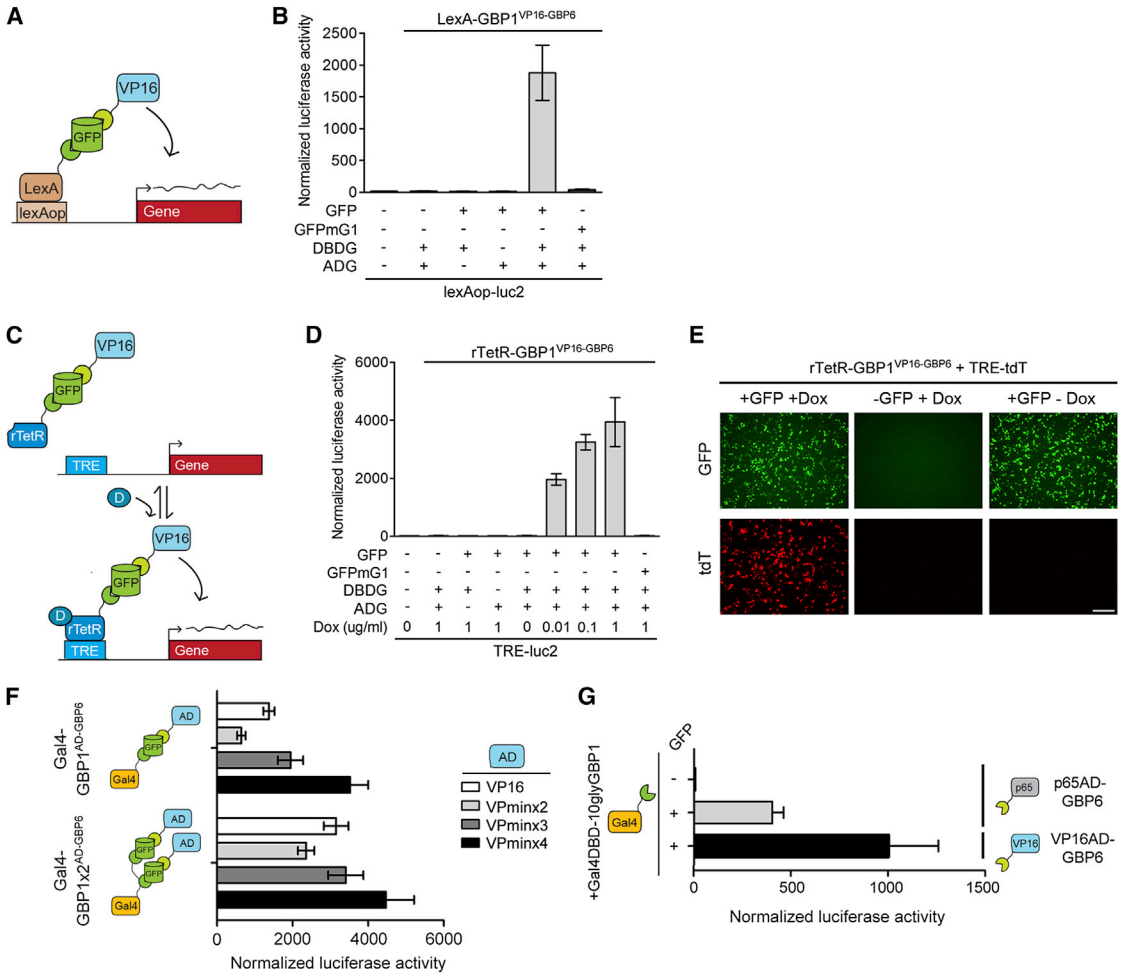

Figure 3. T-DDOGs Are Highly Adjustable

(A–E) T-DDOGs based on LexA (A) and rTetR (C) DBDs. Doxycycline is "D" in (C). TRE includes seven tetO sequences (C). (B) LexA-GBP1$^{VP16\text{-}GBP6}$ activated a lexAop-luc2 reporter only in the presence of GFP. n = 9. (D) rTetR-GBP1$^{VP16\text{-}GBP6}$ activated TRE-luc2 in a GFP- and doxycycline-dependent manner. n = 6–9. (E) Similar results were seen with TRE-tdT. Doxycycline was used at 1 μg/ml. Images were taken 16 hr posttransfection.

(F and G) Tuning T-DDOGs with adjustable DBDs and ADs. (F) Increasing the number of GBP1 on Gal4DBD (n = 6–9) enhanced the transcriptional potency for each ADG (n = 9). (G) Potency of p65AD compared to VP16AD. T-DDOGs used are Gal4-GBP1$^{p65\text{-}GBP6}$ and Gal4-GBP1-B$^{VP16\text{-}GBP6}$. n = 9. Scale bar, 100 μm. Plots are mean ± SD.

of GBPs fused to the DBD (Figure 3F). We further isolated potent T-DDOGs bearing the p65AD (Schmitz and Baeuerle, 1991), an alternative to VP16AD in synthetic transcription systems (Rivera, 1998) (Figure 3G). Overall, we consistently isolated potent T-DDOG variants using the GBP1+6 and GBP2+7 combinations, suggesting that these pairs can effectively recruit various combinations of fusion partners onto the GFP scaffold.

The GFP-Dependent Transcription System Can Be Used in the Mouse for Cell-Specific Gene Regulation

To evaluate whether GFP can control the activity of T-DDOGs in vivo, we used electroporation to introduce GFP, T-DDOGs, and UAS-tdT into the murine retina. In our initial tests, we found that overexpression of VP16AD caused mispositioning of rod photoreceptors in the outer nuclear layer (ONL), likely due to squelching of transcription machinery (Figure S3) (Gill and Ptashne, 1988). To address this, we screened T-DDOGs with alternative ADs described above for their effects in the retina (Extended Experimental Procedures). We found that T-DDOGs made with VPminx2 and p65 ADs induced little to no disruption of normal rod positioning in the ONL (Figure S3). T-DDOGs bearing p65ADs were used in all subsequent experiments.

We examined how T-DDOG activity would respond to changes in GFP expression in the retina (Figures 4, S4, and S5 and Tables S3, S4, S5, and S6). When GFP was expressed under the broadly active CAG promoter, UAS-tdT was induced in GFP-expressing cell types of both the ONL and inner nuclear layer (INL) (Figure 4C). In contrast, little to no tdT signal was detected in electroporated retinas when GFP was excluded (Figures 4C and S4B). When the GFP expression pattern was manipulated with promoters specifically active in rods (Rho-GFP) (Matsuda and Cepko, 2004) or in ON bipolar cells (mGluR6-GFP) (Kim

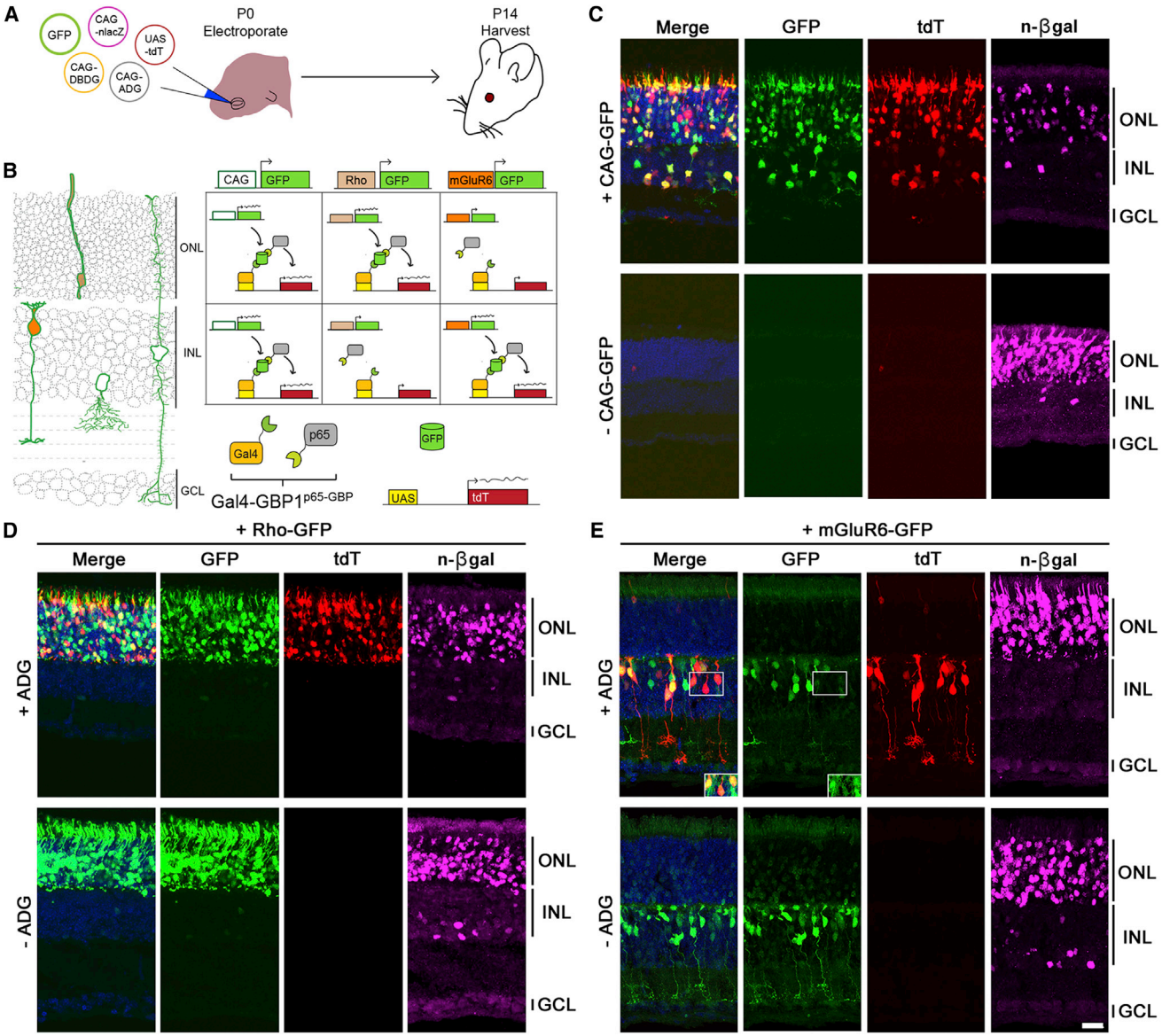

Figure 4. GFP Controls the Spatial Expression of Genes In Vivo

(A) Schematic of experiment.

(B and C) (B) (Left) In electroporated retinas, CAG-GFP expresses in multiple cell types (green outline). Rho-GFP expresses in photoreceptors of the ONL (beige fill). mGluR6-GFP expresses in ON bipolar cells of the INL (orange fill). GCL, ganglion cell layer. (Right) Anticipated UAS-tdT expression pattern aligned to left diagram (C) Gal4-GBP1$^{p65\text{-}GBP6}$ induces UAS-tdT only in the presence of GFP. n-βgal (magenta) is an electroporation marker.

(D and E) (Top) Rho-GFP and mGluR6-GFP induce tdT expression in rods and ON bipolar cells, respectively. (Bottom) tdT activation depends on ADG. Inset of (E) shows GFP and tdT colocalization upon GFP intensity enhancement. Merge panels includes GFP, tdT, and DAPI channels. Scale bar, 20 μm.

See also Figures S3, S4, and S5 and Tables S3, S4, S5, and S6.

et al., 2008), the tdT expression pattern shifted accordingly and was highly restricted to GFP-expressing cells (Figures 4D, 4E, S4, and S5). Cells labeled by the electroporation marker, nuclear β-galactosidase (n-βgal), but not GFP, did not express tdT (Figures 4C–4E). The efficiency of UAS-tdT activation, adjusting for the probability of a cell receiving all four necessary components for tdT activation, was ~56%–93%. Despite the lack of GFP signal amplification with antibodies, more than 90% to 95% of tdT-positive cells were positive for GFP expression in all cases (Table S6). Unexpectedly, we detected faint mGluR6-GFP expression in the ONL, which was not seen without the introduction of T-DDOGs. This low level of GFP induced little to no tdT expression (Figures 4E and S4G). Follow-up experiments indicated that Gal4-GBP1$^{p65\text{-}GBP6}$, but not Gal4-GBP2$^{p65\text{-}GBP7}$, stabilized a low level of ONL GFP leaking from the mGluR6 promoter (see Supplemental Information). This suggests that

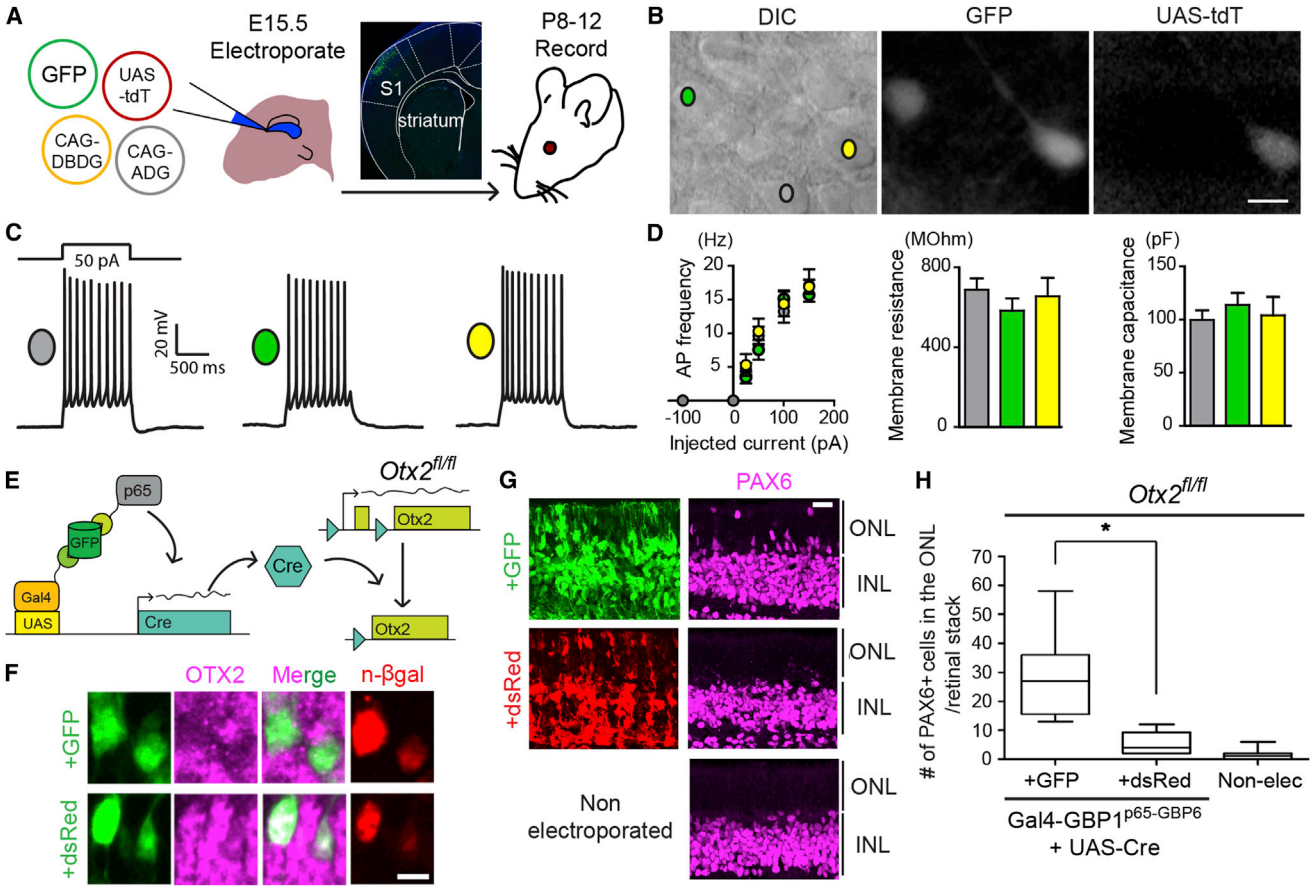

Figure 5. T-DDOGs Support Electrophysiological and Gene Perturbation Studies in the Central Nervous System

(A) Electroporation setup for neuronal recordings. Micrograph shows GFP in electroporated primary somatosensory cortex (S1).

(B–D) (B) Image of an acute brain slice from an electroporated mouse. Scale bar, 10 μm. Three categories of pyramidal layer 2/3 S1 neurons were recorded from brain slices: nonfluorescent controls (gray), GFP+ (green), and GFP+/tdT+ (yellow). (C) Representative single current-clamp trace of action potentials in response to a 50 pA, 1,000-ms-long step current injection. (D) Plots show action potential (AP) frequency upon current injection, as well as input resistance and membrane capacitance of recorded cell classes. $p > 0.5$ for all comparisons (n = 8–10 neurons per condition). Plots show mean ± SEM.

(E–H) GFP-dependent excision of *Otx2*$^{fl/fl}$ in the retina. (E) P0, *Otx2*$^{fl/fl}$ mouse retina was electroporated with T-DDOG components and UAS-Cre and either CAG-GFP or CAG-dsRed. (F–H) (F) Loss of OTX2 was confirmed by OTX2 immunostaining and (G and H) ectopic PAX6+ ONL cells. n = 10 stacks, 5 retinas per electroporated condition. For nonelectroporated retina, n = 19 stacks, 10 retinas. Boxplots show median, maximum, and minimum values. Retinal stacks are 12-μm-thick confocal images. *$p < 0.001$. n-βgal marks electroporated cells in (F). Scale bar, 5 μm in (F) and 20 μm in (G and H).

See also Figures S6 and S7 and Table S7.

Gal4-GBP1$^{p65\text{-}GBP6}$ can reveal GFP expression that is normally below the threshold of detection, whereas Gal4-GBP2$^{p65\text{-}GBP7}$ allows for gene manipulation without revealing subdetection levels of the native GFP expression pattern. Overall, these results showed that GFP could be used as a cell-specific regulator of T-DDOG activities in the mouse.

Utility of GFP-Dependent Transcription System for Electrophysiological Studies and Gene Perturbations

To evaluate whether T-DDOGs altered the properties of neurons, we electroporated GFP, T-DDOGs, and UAS-tdT into the somatosensory cortex and examined various properties of cortical neurons from ~1.5-week-old mouse brains. We compared pyramidal neurons expressing the full set of T-DDOGs, showing both GFP and tdT, with those that expressed GFP alone, as well as with neighboring neurons that lacked fluorescence (Figures 5A–5D). TdT signal was not observed in GFP-negative neurons in the acute slices (data not shown). We found that excitability and passive membrane properties were similar for the three groups of neurons (Figures 5C–5D and Table S7) and were consistent with intrinsic cellular properties previously reported for cortical neurons of this age (Oswald and Reyes, 2008). Moreover, transducing T-DDOGs did not impact morphological features such as dendritic spine density and length (Figure S6 and Table S7). Thus, T-DDOGs are compatible with electrophysiological assays and do not induce functional and structural alterations in the developing brain, within the tested time frame.

We further evaluated the utility of T-DDOGs for deriving biological effects in developing tissues. *Otx2* is a homeobox gene that is necessary for photoreceptor specification in the retina (Nishida et al., 2003). We used GFP to induce Cre-mediated

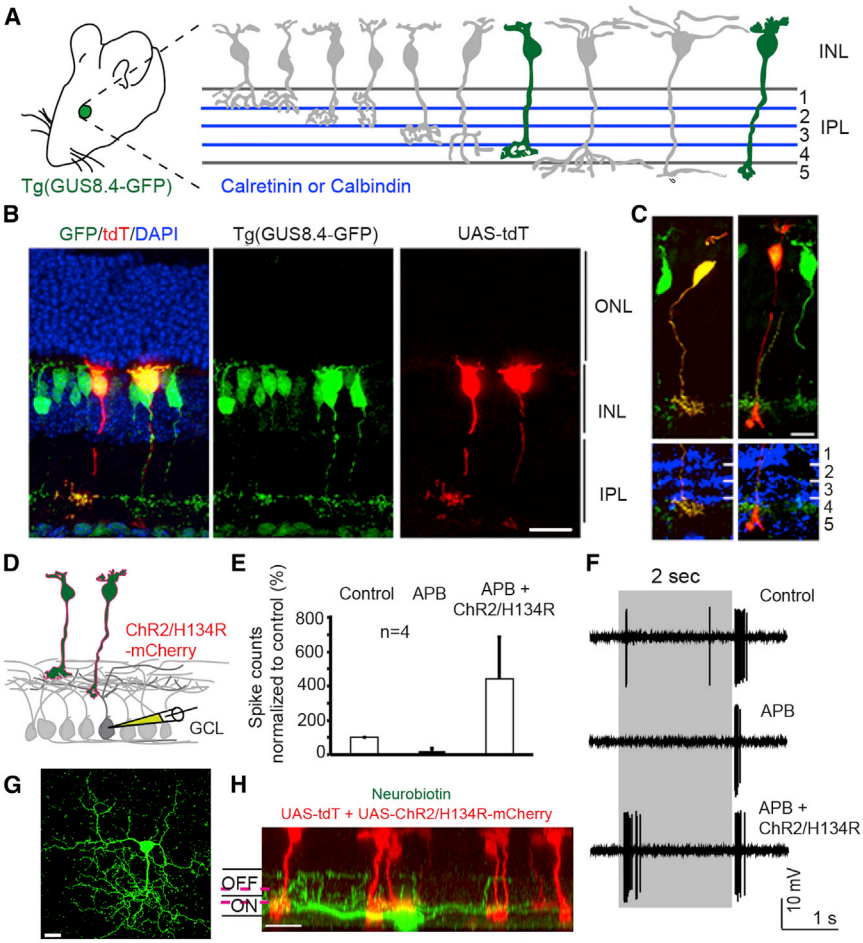

Figure 6. Retrofitting a Transgenic GFP Mouse Line for GFP-Dependent Manipulation of Gene Expression and Neural Circuit Activities

(A) Tg(GUS8.4GFP) expresses GFP in type 7 cone bipolar and rod bipolar cell types (green fill) of the retina. Adopted schematic (Ghosh et al., 2004).

(B) Cryosection of electroporated Tg(GUS8.4GFP) retina expressing Gal4-GBP2$^{p65\text{-}GBP7}$ and UAS-tdT. Scale bar, 20 μm.

(C) Type 7 (left) and rod bipolar (right) cell types labeled by UAS-tdT. Anti-Calretinin (left) or anti-Calbindin (right) staining identify specific layers of the IPL. Scale bar, 10 μm. GFP was immunostained in (B and C).

(D) Schematic of ChR2 experiment. Electroporated Tg(GUS8.4-GFP) retinas expressing 10× UAS-ChR2/H134R-mCherry and 5×UAS-tdT were analyzed for ChR2-mediated responses in random GCL cells.

(E) Cumulative plot of ON responses in GCL cells. Number of spikes counted during the first 300 ms after stimulus onset, normalized to control (minus APB). APB blocks ON responses originating from photoreceptors. Plots are mean ± SEM (n = 4 per condition).

(F) Spiking response of a GCL cell. Gray bar, duration of light stimulus. Response to normal light stimuli under control condition (top) or in the presence of APB (middle). Light stimuli focused on INL activate ChR2/H134R in the presence of APB (lower).

(G and H) Top and side views of a neurobiotin-filled (green) ganglion cell identified by light stimulation of ChR2. Magenta lines indicate level of anti-Chat bands (not shown). Scale bar, 20 μm.

excision of a floxed *Otx2* allele (*Otx2*$^{fl/fl}$) (Tian et al., 2002) in mouse retinas ex vivo, with Cre being under the regulation of the UAS promoter (Figures 5E–5H). This led to the loss of OTX2 protein and the expected ectopic gain of PAX6 in the ONL (Nishida et al., 2003) (Figures 5F and 5G). Conversely, OTX2 levels were not significantly perturbed when GFP was replaced in the same experiment with dsRed (Figure S7). A slight increase in PAX6+ ONL cells above background values was likely due to leakage of UAS-Cre under experimental conditions. Thus, T-DDOGs will be useful for converting GFP expression into desired Cre-mediated genetic changes using a variety of existing conditional alleles. Taken together, these results showed that T-DDOGs are suitable for gene perturbations in the mouse and are compatible with assays of cellular function.

Retrofitting Transgenic GFP Lines for GFP-Dependent Manipulation of Genes and Neural Circuits

We examined whether T-DDOGs can retrofit transgenic GFP lines for cell-specific gene manipulations. In the mouse retina, visual information detected by rod and cone photoreceptors is transmitted to bipolar cells and ultimately to ganglion cells. Among bipolar cells, the rod bipolar cell type receives input from rods, whereas many types of cone bipolar cells receive input primarily from cones. Currently, almost none of the cone bipolar types can be singly isolated for genetic manipulation, but multiple GFP lines do label subsets of bipolar types (Siegert et al., 2009; Wässle et al., 2009). The α-gustducin-GFP transgenic line, Tg(GUS8.4-GFP) (Huang et al., 2003), expresses GFP in type 7 cone bipolar cells and in rod bipolar cells (Figure 6A). Both cell types respond to light increments and are called ON bipolar cells. Introduction of T-DDOGs and UAS-tdT into Tg(GUS8.4-GFP) retinas resulted in tdT induction selectively in these two cell types; identification was based on morphology and axonal stratification in the inner plexiform layer (IPL), aligned to the IPL markers Calbindin or Calretinin (Ghosh et al., 2004) (Figures 6A–6C). Importantly, 98.9% of tdT+ cells were positive for GFP expression (n = 91 cells, sampled from three retinas).

One exciting use of T-DDOGs would be to express light-sensing ion channels in cell types labeled by transgenic GFP for refined, optogenetic probing of neural circuits (Yizhar et al., 2011). We explored this possibility by expressing a UAS-regulated channelrhodopsin-2 (ChR2) variant, H134R (Nagel et al., 2005) in Tg(GUS8.4-GFP)-labeled cells. We asked whether light-driven ChR2 activation in GFP-labeled bipolar cells could trigger downstream spiking responses in cells of the ganglion cell layer (GCL) (Figure 6D). Electroporated retinas were

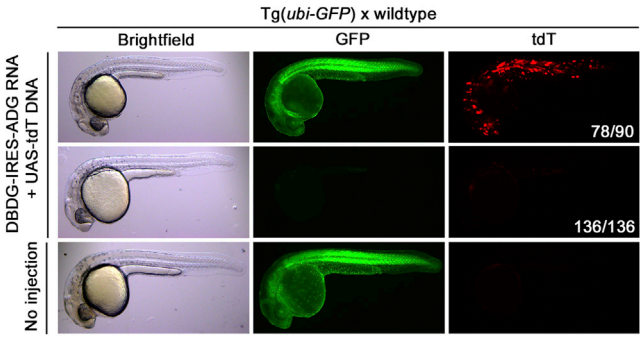

Figure 7. GFP-Dependent Transcription in Transgenic Zebrafish

Embryos from Tg(*ubi-GFP*) × wild-type outcrosses were microinjected with DBDG-IRES-ADG (Gal4-GBP1$^{p65\text{-}GBP6}$) RNA and UAS-tdT DNA at the one- to two-cell stage and examined 1 to 2 days postfertilization. Images represent X number of embryos out of Y number of injected embryos (X/Y), shown in white font in tdT panel.

presented with two different light stimuli, and recordings were performed on GCL cells. The first stimulus had low light intensity and could evoke photoreceptor-mediated responses in GCL cells but was not bright enough to activate ChR2. We used this stimulus to select GCL cells that responded to both light increments and decrements (ON/OFF cells) (Figures 6E and 6F). We next blocked synaptic communication between photoreceptors and ON bipolar cells with 2-amino-4-phosphonobutyrate (APB) (Slaughter and Miller, 1981) and presented the retina with a brighter light stimulus that could activate ChR2. Because ON/OFF GCL cells receive excitatory input from ON bipolar cells, some of these cells should be connected via excitatory synapses (directly or indirectly) to ChR2-expressing ON bipolar cells. Indeed, the brighter stimulus elicited ON responses in some recorded GCL cells in the presence of APB (Figures 6G and 6H). In contrast, recordings made from ON and ON/OFF GCL cells in nonelectroporated regions of multiple retinas did not reveal any response after the onset of the brighter stimulus in the presence of APB (data not shown). Thus, ChR2 activation in rod bipolar or ON cone bipolar cells was robust enough to evoke neurotransmitter release from bipolar cells. Further, the resulting current in GCL cells was large enough to reach spike threshold and evoke spiking responses. These results showed that T-DDOGs could turn on optogenetic tools in transgenic GFP cells, permitting functional interrogation of neural circuits.

Utility of T-DDOGs in Zebrafish

In order to determine whether T-DDOGs can direct GFP-dependent activities in other organisms, zebrafish were tested. Here, T-DDOG components were translated from one bicistronic transcript by linking DBDG and ADG components with an internal ribosome entry site (IRES) element. We microinjected RNAs with this structure into ubiquitin-GFP transgenic (Tg(*ubi-GFP*) (Mosimann et al., 2011) zebrafish embryos in a transient reporter assay. Indeed, mosaic UAS-tdT expression was clearly induced in 78 of 90 injected GFP+ embryos, but not in the 136 injected GFP− embryos (Figure 7). This demonstrates the utility of this system across species.

DISCUSSION

Fluorescent proteins are useful for illuminating cells and cellular processes. Moreover, their apparent lack of connection to many host protein networks makes them ideal scaffolds upon which one can build synthetic complexes with desirable biological activities. We demonstrated this principle here by using GFP to induce formation of a hybrid transcription factor for gene regulation purposes. The ability to use GFP for gene regulation now enables one to experiment with many GFP-labeled cell types without the need to create new cell-specific driver lines or to discover new cell-specific promoters. This system can be used for gene overexpression and gene deletion (Figures 4, 5, 6, and 7) and should be able to perform RNA interference (RNAi) knockdown (Dickins et al., 2007; Dietzl et al., 2007). Activities of the system can be controlled by GFP and its derivatives, but not by red fluorescent proteins, thereby allowing the two types of fluorescent proteins to be used independently in the same experiment. Red fluorescent proteins can likely be used as scaffolds as well. In particular, monomeric variants such as mCherry would be straightforward to use, as they do not undergo obligate dimerization or tetramerization (Campbell et al., 2002).

Selective Control of GFP-Labeled Cells in Transgenic GFP Organisms

The development and functions of complex multicellular organisms depend upon the activities of a large number of distinct cell types. To investigate these activities in the nervous system, for example, many molecular tools have been developed for anatomical circuit tracing, as well as physiological control (Wickersham and Feinberg, 2012; Yizhar et al., 2011). However, the full potential of these tools can only be realized when one can selectively control them in any cell type in the nervous system. We demonstrated that the diverse transgenic GFP lines available in the mouse and other organisms would be useful for cell-specific manipulation of genes and neural circuits. In the mouse, such manipulations are performed primarily with recombinases such as Cre. Although we anticipate that the number of cell-specific Cre mouse lines will continually increase along with that of GFP lines, each collection of lines will be independently useful for some applications and will be complementary for other applications. As discussed below, the use of GFP is not necessarily limited to transcriptional control. Nevertheless, gene regulatory systems based on transcription factors differ fundamentally from those based on recombination strategies. As recombination induces alterations to DNA sequences, this typically results in permanent changes in gene expression. In contrast, transcription systems are reversible. Recombination systems are especially useful for targeting cells with a common gene expression history and for long-term transgene expression independent of initial induction signals. However, the irreversibility of recombination events can result in the manipulation of undesired cell types. This should be less of a problem for a transcription system, as continual expression of GFP, in our case, is required to maintain the transcription of target genes. Although GFP may persist for a prolonged period of time after its own transcription has been shut off, this effect may be advantageous in certain applications, such as when it is desirable to achieve a

moderately prolonged but reversible gene expression effect. When temporal control of gene expression is desired regardless of GFP expression, rTetR-based T-DDOGs should be useful as they are additionally controlled by drug treatment (Figures 3C–3E) and could take advantage of the various TRE reagents available (Schönig et al., 2010).

There are additional reasons to use GFP lines for cell-specific targeting. First, not all definable cell types can be specifically targeted by a single driver line (Dymecki et al., 2010). Restriction of target gene expression may be accomplished by intersecting GFP expression with expression of T-DDOG components, other transcription systems, and/or recombination systems. Second, position effects can sometimes unexpectedly activate GFP in unique cell types. For example, this is thought to be the case for the Tg(GUS8.4-GFP) line and the Tg(Thy1-XFP) collections (Huang et al., 2003; Feng et al., 2000). Replacement of transgenes typically requires the generation of new transgenic lines and can result in changes to cell specificity of transgene expression. Emerging site-specific, genome-editing strategies hold promise for enabling efficient swapping of transgenes while minimizing changes to cell specificity (Cong et al., 2013; Gohl et al., 2011; Mali et al., 2013). However, it still takes a relatively long time, as well as significant expense, to generate, characterize, and maintain modified transgenic mouse lines.

The GFP-dependent transcription system should find applications beyond mice and zebrafish. As T-DDOGs are built from protein parts commonly used in other model organisms such as *Drosophila*, other communities can easily adopt T-DDOG components for use in concert with existing GFP driver and responder lines, as well as transient gene delivery vectors. In addition, the modularity of this system allows for a seemingly unlimited number of T-DDOGs to be created according to user demands. Notably, T-DDOGs with customizable DNA-binding specificity (Hsu and Zhang, 2012) would allow for targeted control of endogenous loci without the need for responder cassettes.

Practical Considerations for T-DDOG Use

Although T-DDOG activities are highly dependent on GFP expression, whether one succeeds in converting an observed GFP expression pattern into corresponding gene output pattern depends on several factors. First, cells expressing GFP at low levels, or transiently, may evade detection in the initial stages of characterization. Such ''background'' GFP expression may be detected by certain T-DDOG configurations. Differing fusion protein stability and/or differing GBP affinity for GFP probably contribute to differences in T-DDOG sensitivity. Specifically, we found that Gal4-GBP1$^{p65\text{-}GBP6}$ promoted detection of normally undetectable GFP expression from mGluR-GFP in photoreceptors. However, little to no T-DDOG-mediated expression occurred in these cells. As an mGluR6-driven Cre construct was found to induce recombination in photoreceptors, in addition to bipolar cells (data not shown), we interpret the photoreceptor GFP signal as reflecting leakage from the mGluR6 promoter, as well as stabilization of the leaky GFP by Gal4-GBP1$^{p65\text{-}GBP6}$. Because Gal4-GBP2$^{p65\text{-}GBP7}$ did not reveal the leaky mGluR6-GFP expression and its corresponding T-DDOG did not induce reporter output in photoreceptors, Gal4-GBP2$^{p65\text{-}GBP7}$ may be used for cases when it is not desirable to reveal GFP expression normally below detection threshold. A second issue regards T-DDOG detection of transient GFP expression during early development. This could be addressed by using rTetR-based T-DDOGs for temporal control or by restricting T-DDOGs expression to late progenitors or postmitotic cells, as is possible with electroporation, viral vectors, and/or late-expressing promoters.

Very high levels of GFP expression also require consideration, as too much GFP may saturate GBP binding sites, thereby preventing assembly of T-DDOGs (Figure 2E). Nonetheless, we could induce strong T-DDOG readout in Tg(CRX-GFP), a very strong GFP-expressing mouse line (Samson et al., 2009) (data not shown). When necessary, there are approaches to overcome the issue of excessive GFP expression. First, one can capture T-DDOG activity using a recombinase as the T-DDOG readout. We demonstrated that T-DDOGs could drive expression of Cre to induce irreversible gene expression changes regardless of changes in GFP level. Second, we showed that one could increase the number of GBPs on the DBDG component; this is expected to enhance the GFP binding capacity of the system. Lastly, higher levels of expression of T-DDOGs should be able to balance high GFP levels. Transgenic lines expressing T-DDOGs at high, medium, and low levels should be sufficient for a research community to manipulate a broad range of transgenic GFP lines.

Here, we demonstrated that electroporation or microinjection could immediately be used to deliver T-DDOGs to receptive tissues and organisms for manipulation of GFP-labeled cell types. Additionally, it should require little effort to extend the delivery route to viral vectors. The two components of T-DDOGs can be linked by IRES elements or 2a peptides for expression from a single promoter (Figure 7). Each component is relatively small, ranging from ~500 bp to ~1.2 kbp in length, allowing both T-DDOG components to fit into popular viral vectors such as adeno-associated viruses (AAVs) (Yizhar et al., 2011). Responder cassettes can also be delivered virally or by electroporation (Figures 4, 5, and 6). Transient delivery methods usually do not provide access to all possible cell types within a tissue or organism; this can be taken into account during experimental design. For example, any retinal cell class is accessible given the right choice of AAV serotypes or electroporation method (Matsuda and Cepko, 2004, 2007; Watanabe et al., 2013). Furthermore, the inherent cell-type specificity of certain gene delivery methods can be exploited to subtract undesired GFP-labeled cell types from being manipulated. For some applications, it will be desirable to deliver T-DDOGs to all cells in a tissue, or to entire organisms. Transgenic lines expressing T-DDOGs under the control of broadly active promoters would meet these needs, and these tools are under development.

Whenever exogenous components are delivered to cells, one should be cautious of unintended effects. Potential side effects from AD overexpression have long been recognized (Gill and Ptashne, 1988), but applications with transcription factors continue to grow (Schönig et al., 2010; Venken et al., 2011) and drive meaningful discoveries (Kinoshita et al., 2012; Miyamichi et al., 2011). As we found here, problems with an AD may be overcome by testing ADs differing in origin and transcriptional

potency. Alternatively, one can reduce expression of a given T-DDOG. IRES-linked cassettes typically give lower expression of genes in the second position relative to those in the first position (Mizuguchi et al., 2000). This could be used to express the DBDG component at high levels while keeping the ADG levels relatively low.

Fluorescent Proteins as Multifunctional Switches for Heterologous Systems

As GFP does not have any committed regulatory function in host cells, it may be co-opted for other regulatory purposes. To realize GFP's full potential, additional GFP-binding reagents and engineering efforts will be needed to expand its functionality and to improve the performance of GFP-dependent devices. Beyond transcription, the GFP scaffold should be able to regulate other activities such as recombination (Jullien et al., 2003) and proteolysis (Wehr et al., 2006). Although the GBP1 binding epitope on GFP has been revealed by X-ray crystallography (Kirchhofer et al., 2010), it is unclear how GBP2, 6, or 7 bind to GFP. Structural understanding of how GBP pairs co-occupy GFP would facilitate the design of other GFP-inducible complexes, such as when protein fragments have to be positioned in strict orientations.

Eventually, fluorescent proteins may become preferred transgenes for organisms with long generation times, such as rodents and primates. Because the expression pattern of fluorescent proteins can be characterized from the first set of transgene carriers, any experimental manipulation of labeled cells could be conducted within the same generation by transient device delivery or in the next generation by mating with transgenic device carriers. Also, as one can retroactively build systems to exploit fluorescent proteins for different purposes, it may become unnecessary to generate redundant lines driving different transgenes selectively in the same cell populations. Lastly, engineering of small-molecule ligands that regulate fluorescence would even enable one to use fluorescent proteins exclusively for gene control without interfering with the imaging of other spectrally overlapping probes (Kumagai et al., 2013).

Perspective on Targeting Intracellular Products for Cell-Specific Control

Many intracellular products, such as RNA and proteins, are expressed in a cell-specific manner and could potentially be exploited as spatial signals to control synthetic circuits in multicellular organisms. Here, we demonstrated that artificially derived binding proteins are useful for co-opting an intracellular protein, GFP, for this purpose. Because this approach does not require any modification of the target molecule or rely on the molecule's natural interactions or functions, it may be generalizable to any intracellular product for which artificially derived binding proteins can be selected. Certainly, GFP seems to be an ideal target because it is an exogenous molecule that shows little connection to host protein networks. However, other exogenous molecules, such as β-galactosidase or Cre recombinase, should also be useful as scaffold proteins. Furthermore, endogenous molecules probably exhibit a spectrum of connectivity within the host interactome, and a subset might be appropriate for conferring cell-specific manipulations in multicellular organisms. The ability to use intracellular products simply as cell-specific scaffolds would enhance one's ability to target and control cells in nonmodel organisms where transgenic lines are not available.

EXPERIMENTAL PROCEDURES

Detailed methods, data analysis, and reagents used can be found in the Extended Experimental Procedures.

Animals

All animal experiments performed were approved by the Institutional Animal Care and Use Committee at Harvard University. Animal information is in the Extended Experimental Procedures.

Molecular Biology and Screens

Using standard techniques, coding sequences of GBPs were fused to those of DBDs or ADs in many configurations, and the products were inserted into pCAG (Niwa et al., 1991). Pairwise combination of DBDG and ADG constructs were then introduced into 293T cells or the mouse retina for screens. See the Extended Experimental Procedures for details.

In Vitro Luciferase Assays

Plasmids encoding CAG-driven GFP, DBDG, and ADG were transfected via polyethyleneimine (PEI) into 293T cells along with plasmids encoding UAS-luc2 and Renilla luciferase or UAS-tdT. Cells were harvested 24 hr later for dual-luciferase assay (Promega) or imaged 16 hr later. All transfections except for the dosage curve were done at a 1:1:1 (GFP:DBDG:ADG) plasmid molar ratio.

In Vivo Electroporations

P0 CD1 retinas were microinjected with plasmids into the subretinal space and subjected to electroporation (Matsuda and Cepko, 2004). Plasmids encoded DBDG, ADG, CAG-nlacZ (expresses the electroporation marker n-βgal), UAS-tdT, and different promoter-GFP constructs. Electroporated retinas were harvested at P14, immunostained for n-βgal, and imaged by confocal microscopy. At P3–5, Tg(GUS8.4GFP) retinas were electroporated with plasmids encoding T-DDOG components, UAS-driven constructs, and CAG-nlacZ; retinas were harvested between 3 and 4 weeks of age for UAS-tdT detection and between 8 and 10 weeks of age for 10×UAS-ChR2/134R stimulation. Wherever applicable, retinas were immunostained with anti-GFP or anti-dsRed to visualize processes. Anti-Calbindin or anti-Calretinin label layers in the IPL.

Neuronal Recordings

C57BL/6 embryos were electroporated with plasmids encoding CAG-driven GFP, DBDG, ADG, and UAS-tdT into the lateral ventricle at embryonic day 15.5. Acute brain slices were prepared from electroporated 1- to 2-week-old mice using standard procedures. Whole-cell current clamp recordings were performed on GFP−, GFP+, and GFP+/tdT+ cortical layer 2/3 pyramidal neurons in regions of dense electroporation. For ChR2/H134R experiment, electroporated retinas from 8- to 10-week-old Tg(GUS8.4GFP) mice were flat mounted, and loose cell-attached patch clamp was performed on GCL cells that had mCherry/tdT+ bipolar cells in their dendritic fields. Photoreceptors were stimulated by light focused on the outer segments of photoreceptors at a light intensity of 1.3×10^3 R*/s. 20 μM APB was used whenever applicable. ChR2 was stimulated by light focused on the bipolar cell layer at $\sim 10^8$ R*/s for 2 s. Epifluorescence or two-photon microscopes were used to identify fluorescent cells.

Otx2 Removal Experiment

P0 $Otx2^{fl/fl}$ (Tian et al., 2002) retinas were electroporated ex vivo (Emerson and Cepko, 2011) with plasmids bearing Gal4-$GBP1^{p65\text{-}GBP6}$, UAS-Cre, and CAG-nlacZ along with either GFP or dsRed-expressing plasmids. Retinas were cultured ex vivo, harvested at P8, immunostained for OTX2, PAX6, and/or n-βgal expression, and subjected to confocal imaging.

Zebrafish Microinjections

DBDG and ADG coding sequences of Gal4-$GBP1^{p65\text{-}GBP6}$ were linked by an IRES element, subcloned into pCS2+, and transcribed in vitro from the SP6

promoter (mMessage mMachine SP6 RNA Kit, Ambion). RNAs were subjected to LiCl precipitation. One- to two-cell embryos were injected with 40 ng/μl RNA encoding IRES-linked T-DDOG and 25 ng/μl of NotI-linearized UAS-tdT DNA. GFP+ and GFP− embryos, obtained from outcrosses of heterozygote Tg(*ubi-GFP*) (Mosimann et al., 2011) males to wild-type Tubingen females, were blindly injected with the same RNA/DNA mixture in the same experiment such that the injection success rate for both genotypes should be similar. Injected embryos were incubated at 28°C, and survivors were analyzed for GFP and tdT expression 1 to 2 days postfertilization.

Statistical Analysis

Two-tailed Student's t test assuming unequal variance was used for all comparisons except cortical recording analysis, for which one-way ANOVA was used. $p > 0.05$ is judged as statistically significant.

See the Supplemental Information for detailed methods and reagents used.

SUPPLEMENTAL INFORMATION

Supplemental Information includes Extended Experimental Procedures, seven figures, and seven tables and can be found with this article online at http://dx.doi.org/10.1016/j.cell.2013.07.021.

ACKNOWLEDGMENTS

We thank Matt Harris and Katrin Henke for assistance with zebrafish injections; Mark Emerson for discussions of *Otx2* experiment; Quentin Gilly of Perrimon lab for access to microplate reader; James deMelo for help with mouse transfer; Tim Cherry for contributing to illustrations; and Kailun Jiang, Jonathan Coleman, Susan Dymecki, Jacob Hodgson, Douglas Allan, Andreas Mayer, Jesse Gray, Michael Springer, Kevin Struhl, Ben Huang, and members of the Cepko/Tabin/Dymecki lab for comments. We are grateful to Heinrich Leonhardt and Ulrich Rothbauer for advice and GBP reagents. We thank Liqun Luo, David Bartel, Gerald Rubin, Benjamin White, Dominic Esposito, Warner Greene, and Matija Peterlin for plasmids from Addgene, Robert Margolskee for Tg(GUS8.4GFP) line, and Leonard Zon for Tg(*Ubi-GFP*) line. Y.K. was supported by the Leonard and Isabelle Goldenson Research Fellowship. B.R. was supported by a European Research Council grant, a Swiss-Hungarian grant, and TREATRUSH, SEEBETTER, and OPTONEURO grants from the European Union. C.L.C. and B.L.S. were supported by the Howard Hughes Medical Institute.

Received: October 31, 2012
Revised: May 31, 2013
Accepted: July 15, 2013
Published: August 15, 2013

REFERENCES

Baron, U., Gossen, M., and Bujard, H. (1997). Tetracycline-controlled transcription in eukaryotes: novel transactivators with graded transactivation potential. Nucleic Acids Res. *25*, 2723–2729.

Butala, M., Zgur-Bertok, D., and Busby, S.J. (2009). The bacterial LexA transcriptional repressor. Cell. Mol. Life Sci. *66*, 82–93.

Campbell, R.E., Tour, O., Palmer, A.E., Steinbach, P.A., Baird, G.S., Zacharias, D.A., and Tsien, R.Y. (2002). A monomeric red fluorescent protein. Proc. Natl. Acad. Sci. USA *99*, 7877–7882.

Caussinus, E., Kanca, O., and Affolter, M. (2012). Fluorescent fusion protein knockout mediated by anti-GFP nanobody. Nat. Struct. Mol. Biol. *19*, 117–121.

Chalfie, M., Tu, Y., Euskirchen, G., Ward, W.W., and Prasher, D.C. (1994). Green fluorescent protein as a marker for gene expression. Science *263*, 802–805.

Chang, A.L., Wolf, J.J., and Smolke, C.D. (2012). Synthetic RNA switches as a tool for temporal and spatial control over gene expression. Curr. Opin. Biotechnol. *23*, 679–688.

Cong, L., Ran, F.A., Cox, D., Lin, S., Barretto, R., Habib, N., Hsu, P.D., Wu, X., Jiang, W., Marraffini, L.A., and Zhang, F. (2013). Multiplex genome engineering using CRISPR/Cas systems. Science *339*, 819–823.

Culler, S.J., Hoff, K.G., and Smolke, C.D. (2010). Reprogramming cellular behavior with RNA controllers responsive to endogenous proteins. Science *330*, 1251–1255.

Dickins, R.A., McJunkin, K., Hernando, E., Premsrirut, P.K., Krizhanovsky, V., Burgess, D.J., Kim, S.Y., Cordon-Cardo, C., Zender, L., Hannon, G.J., and Lowe, S.W. (2007). Tissue-specific and reversible RNA interference in transgenic mice. Nat. Genet. *39*, 914–921.

Dietzl, G., Chen, D., Schnorrer, F., Su, K.C., Barinova, Y., Fellner, M., Gasser, B., Kinsey, K., Oppel, S., Scheiblauer, S., et al. (2007). A genome-wide transgenic RNAi library for conditional gene inactivation in Drosophila. Nature *448*, 151–156.

Dymecki, S.M., Ray, R.S., and Kim, J.C. (2010). Mapping cell fate and function using recombinase-based intersectional strategies. Methods Enzymol. *477*, 183–213.

Emerson, M.M., and Cepko, C.L. (2011). Identification of a retina-specific Otx2 enhancer element active in immature developing photoreceptors. Dev. Biol. *360*, 241–255.

Feng, G., Mellor, R.H., Bernstein, M., Keller-Peck, C., Nguyen, Q.T., Wallace, M., Nerbonne, J.M., Lichtman, J.W., and Sanes, J.R. (2000). Imaging neuronal subsets in transgenic mice expressing multiple spectral variants of GFP. Neuron *28*, 41–51.

Ghosh, K.K., Bujan, S., Haverkamp, S., Feigenspan, A., and Wässle, H. (2004). Types of bipolar cells in the mouse retina. J. Comp. Neurol. *469*, 70–82.

Gill, G., and Ptashne, M. (1988). Negative effect of the transcriptional activator GAL4. Nature *334*, 721–724.

Gohl, D.M., Silies, M.A., Gao, X.J., Bhalerao, S., Luongo, F.J., Lin, C.C., Potter, C.J., and Clandinin, T.R. (2011). A versatile in vivo system for directed dissection of gene expression patterns. Nat. Methods *8*, 231–237.

Gong, S., Zheng, C., Doughty, M.L., Losos, K., Didkovsky, N., Schambra, U.B., Nowak, N.J., Joyner, A., Leblanc, G., Hatten, M.E., and Heintz, N. (2003). A gene expression atlas of the central nervous system based on bacterial artificial chromosomes. Nature *425*, 917–925.

Ho, S.N., Biggar, S.R., Spencer, D.M., Schreiber, S.L., and Crabtree, G.R. (1996). Dimeric ligands define a role for transcriptional activation domains in reinitiation. Nature *382*, 822–826.

Hsu, P.D., and Zhang, F. (2012). Dissecting neural function using targeted genome engineering technologies. ACS Chem. Neurosci. *3*, 603–610.

Huang, L., Max, M., Margolskee, R.F., Su, H., Masland, R.H., and Euler, T. (2003). G protein subunit G gamma 13 is coexpressed with G alpha o, G beta 3, and G beta 4 in retinal ON bipolar cells. J. Comp. Neurol. *455*, 1–10.

Jobling, S.A., Jarman, C., Teh, M.M., Holmberg, N., Blake, C., and Verhoeyen, M.E. (2003). Immunomodulation of enzyme function in plants by single-domain antibody fragments. Nat. Biotechnol. *21*, 77–80.

Jullien, N., Sampieri, F., Enjalbert, A., and Herman, J.P. (2003). Regulation of Cre recombinase by ligand-induced complementation of inactive fragments. Nucleic Acids Res. *31*, e131.

Kim, D.S., Matsuda, T., and Cepko, C.L. (2008). A core paired-type and POU homeodomain-containing transcription factor program drives retinal bipolar cell gene expression. J. Neurosci. *28*, 7748–7764.

Kinoshita, M., Matsui, R., Kato, S., Hasegawa, T., Kasahara, H., Isa, K., Watakabe, A., Yamamori, T., Nishimura, Y., Alstermark, B., et al. (2012). Genetic dissection of the circuit for hand dexterity in primates. Nature *487*, 235–238.

Kirchhofer, A., Helma, J., Schmidthals, K., Frauer, C., Cui, S., Karcher, A., Pellis, M., Muyldermans, S., Casas-Delucchi, C.S., Cardoso, M.C., et al. (2010). Modulation of protein properties in living cells using nanobodies. Nat. Struct. Mol. Biol. *17*, 133–138.

Kumagai, A., Ando, R., Miyatake, H., Greimel, P., Kobayashi, T., Hirabayashi, Y., Shimogori, T., and Miyawaki, A. (2013). A bilirubin-inducible fluorescent protein from eel muscle. Cell *153*, 1602–1611.

Luan, H., Peabody, N.C., Vinson, C.R., and White, B.H. (2006). Refined spatial manipulation of neuronal function by combinatorial restriction of transgene expression. Neuron *52*, 425–436.

Mali, P., Yang, L., Esvelt, K.M., Aach, J., Guell, M., DiCarlo, J.E., Norville, J.E., and Church, G.M. (2013). RNA-guided human genome engineering via Cas9. Science *339*, 823–826.

Masland, R.H. (2004). Neuronal cell types. Curr. Biol. *14*, R497–R500.

Matsuda, T., and Cepko, C.L. (2004). Electroporation and RNA interference in the rodent retina in vivo and in vitro. Proc. Natl. Acad. Sci. USA *101*, 16–22.

Matsuda, T., and Cepko, C.L. (2007). Controlled expression of transgenes introduced by in vivo electroporation. Proc. Natl. Acad. Sci. USA *104*, 1027–1032.

Miyamichi, K., Amat, F., Moussavi, F., Wang, C., Wickersham, I., Wall, N.R., Taniguchi, H., Tasic, B., Huang, Z.J., He, Z., et al. (2011). Cortical representations of olfactory input by trans-synaptic tracing. Nature *472*, 191–196.

Mizuguchi, H., Xu, Z., Ishii-Watabe, A., Uchida, E., and Hayakawa, T. (2000). IRES-dependent second gene expression is significantly lower than cap-dependent first gene expression in a bicistronic vector. Mol. Ther. *1*, 376–382.

Mosimann, C., Kaufman, C.K., Li, P., Pugach, E.K., Tamplin, O.J., and Zon, L.I. (2011). Ubiquitous transgene expression and Cre-based recombination driven by the ubiquitin promoter in zebrafish. Development *138*, 169–177.

Nagel, G., Brauner, M., Liewald, J.F., Adeishvili, N., Bamberg, E., and Gottschalk, A. (2005). Light activation of channelrhodopsin-2 in excitable cells of Caenorhabditis elegans triggers rapid behavioral responses. Curr. Biol. *15*, 2279–2284.

Nishida, A., Furukawa, A., Koike, C., Tano, Y., Aizawa, S., Matsuo, I., and Furukawa, T. (2003). Otx2 homeobox gene controls retinal photoreceptor cell fate and pineal gland development. Nat. Neurosci. *6*, 1255–1263.

Niwa, H., Yamamura, K., and Miyazaki, J. (1991). Efficient selection for high-expression transfectants with a novel eukaryotic vector. Gene *108*, 193–199.

Oswald, A.M., and Reyes, A.D. (2008). Maturation of intrinsic and synaptic properties of layer 2/3 pyramidal neurons in mouse auditory cortex. J. Neurophysiol. *99*, 2998–3008.

Pollock, R., and Clackson, T. (2002). Dimerizer-regulated gene expression. Curr. Opin. Biotechnol. *13*, 459–467.

Rivera, V.M. (1998). Controlling gene expression using synthetic ligands. Methods *14*, 421–429.

Rothbauer, U., Zolghadr, K., Tillib, S., Nowak, D., Schermelleh, L., Gahl, A., Backmann, N., Conrath, K., Muyldermans, S., Cardoso, M.C., and Leonhardt, H. (2006). Targeting and tracing antigens in live cells with fluorescent nanobodies. Nat. Methods *3*, 887–889.

Rothbauer, U., Zolghadr, K., Muyldermans, S., Schepers, A., Cardoso, M.C., and Leonhardt, H. (2008). A versatile nanotrap for biochemical and functional studies with fluorescent fusion proteins. Mol. Cell. Proteomics *7*, 282–289.

Sadowski, I., Ma, J., Triezenberg, S., and Ptashne, M. (1988). GAL4-VP16 is an unusually potent transcriptional activator. Nature *335*, 563–564.

Samson, M., Emerson, M.M., and Cepko, C.L. (2009). Robust marking of photoreceptor cells and pinealocytes with several reporters under control of the Crx gene. Dev. Dyn. *238*, 3218–3225.

Schmitz, M.L., and Baeuerle, P.A. (1991). The p65 subunit is responsible for the strong transcription activating potential of NF-kappa B. EMBO J. *10*, 3805–3817.

Schönig, K., Bujard, H., and Gossen, M. (2010). The power of reversibility regulating gene activities via tetracycline-controlled transcription. Methods Enzymol. *477*, 429–453.

Shaner, N.C., Steinbach, P.A., and Tsien, R.Y. (2005). A guide to choosing fluorescent proteins. Nat. Methods *2*, 905–909.

Siegert, S., Scherf, B.G., Del Punta, K., Didkovsky, N., Heintz, N., and Roska, B. (2009). Genetic address book for retinal cell types. Nat. Neurosci. *12*, 1197–1204.

Siegert, S., Cabuy, E., Scherf, B.G., Kohler, H., Panda, S., Le, Y.Z., Fehling, H.J., Gaidatzis, D., Stadler, M.B., and Roska, B. (2012). Transcriptional code and disease map for adult retinal cell types. Nat. Neurosci. *15*, 487–495.

Slaughter, M.M., and Miller, R.F. (1981). 2-amino-4-phosphonobutyric acid: a new pharmacological tool for retina research. Science *211*, 182–185.

Tian, E., Kimura, C., Takeda, N., Aizawa, S., and Matsuo, I. (2002). Otx2 is required to respond to signals from anterior neural ridge for forebrain specification. Dev. Biol. *242*, 204–223.

Trinkle-Mulcahy, L., Boulon, S., Lam, Y.W., Urcia, R., Boisvert, F.M., Vandermoere, F., Morrice, N.A., Swift, S., Rothbauer, U., Leonhardt, H., and Lamond, A. (2008). Identifying specific protein interaction partners using quantitative mass spectrometry and bead proteomes. J. Cell Biol. *183*, 223–239.

Tsien, R.Y. (1998). The green fluorescent protein. Annu. Rev. Biochem. *67*, 509–544.

Venken, K.J., Simpson, J.H., and Bellen, H.J. (2011). Genetic manipulation of genes and cells in the nervous system of the fruit fly. Neuron *72*, 202–230.

Wässle, H., Puller, C., Müller, F., and Haverkamp, S. (2009). Cone contacts, mosaics, and territories of bipolar cells in the mouse retina. J. Neurosci. *29*, 106–117.

Watanabe, S., Sanuki, R., Ueno, S., Koyasu, T., Hasegawa, T., and Furukawa, T. (2013). Tropisms of AAV for subretinal delivery to the neonatal mouse retina and its application for in vivo rescue of developmental photoreceptor disorders. PLoS ONE *8*, e54146.

Wehr, M.C., Laage, R., Bolz, U., Fischer, T.M., Grünewald, S., Scheek, S., Bach, A., Nave, K.A., and Rossner, M.J. (2006). Monitoring regulated protein-protein interactions using split TEV. Nat. Methods *3*, 985–993.

Wickersham, I.R., and Feinberg, E.H. (2012). New technologies for imaging synaptic partners. Curr. Opin. Neurobiol. *22*, 121–127.

Wurch, T., Pierré, A., and Depil, S. (2012). Novel protein scaffolds as emerging therapeutic proteins: from discovery to clinical proof-of-concept. Trends Biotechnol. *30*, 575–582.

Yizhar, O., Fenno, L.E., Davidson, T.J., Mogri, M., and Deisseroth, K. (2011). Optogenetics in neural systems. Neuron *71*, 9–34.

EXTENDED EXPERIMENTAL PROCEDURES

Animals

The following mouse strains were used: Timed pregnant CD1 and C57/BL6 mothers (Charles River Breeding Laboratories, Boston, MA), *Otx2*$^{fl/fl}$ mice (Tian et al., 2002). C57/BL6 mice (Charles River Breeding Laboratories or Jackson Laboratories, Bar Harbor, ME). Tg(GUS8.4GFP) (Huang et al., 1999) (Robert Margolskee, Monell Chemical Senses Center, Philadelphia, PA). Zebrafish strains used are Tubingen wild-type and Tg(*ubi-GFP*) zebrafish (Mosimann et al., 2011) (Leonard Zon, Children's hospital, Boston, MA).

Molecular Biology

GBP Sequences

GBP1 and 4 sequences were obtained from published protein sequence (PDB; 3K1K for GBP1 and 3G9A for GBP4), back-translated, codon-optimized for the mouse and synthesized by Genewiz (New Jersey), generating pUC57-GBP1 and pUC57-GBP4. Plasmids carrying GBPs 2, 5, 6 and 7 were obtained from Ulrich Rothbauer (Ludwig Maximilians University Munich). GBP6 was synthesized based on provided sequence from Ulrich Rothbauer to generate pUC57-GBP6 (Genewiz).

Miscellaneous Plasmids

pCAG-GFP (Addgene plasmid 11150) (Matsuda and Cepko, 2004), pCAG-YFP (Addgene plasmid 11180) (Matsuda and Cepko, 2004), pCAG-CFP (Addgene plasmid 11179) (Matsuda and Cepko, 2004), pCAG-tdT (Cepko lab, Harvard Medical School), pCAG-mCherry (Cepko lab, Harvard Medical School), pCAG-dsRed (Addgene plasmid 11151) (Matsuda and Cepko, 2004), pUAS-luc2 (Addgene plasmid 24343) (Potter et al., 2010), pRL-TK (Promega, #E2241), pBS SK+ (Stratagene), mGluR6 (200bp crit reg)+SV40p-GFP-IRES-AP (referred to as mGluR6-GFP in main text) (Addgene plasmid 18817) (Kim et al., 2008), pRho-GFP-IRES-AP (referred to as Rho-GFP in main text) (Emerson and Cepko, 2011), pCAG-nlacZ (Cepko lab, Harvard Medical School).

Plasmid Construction

pCAG-GFPmG1

To produce GFPmG1, splicing by overlap extension (SOE) PCR was performed to introduce E143K and N147Q mutations in EGFP. The mutagenized PCR product has AgeI-Kozak consensus sequence and NotI on the 5′ and 3′ ends, respectively. Using AgeI/NotI, this fragment was cloned in place of EGFP in the pCAG-GFP vector.

pUAS-tdT

TdT was amplified from pCAG-tdT with EcoRI and XbaI restriction sites added on the 5′ and 3′ ends, respectively. This fragment was cloned into pUAS-luc2 (5xUAS) via EcoRI/XbaI, replacing the luciferase sequence to give pUAS-tdT.

pTRE-tdT and pTRE-luc2

TREtight promoter was amplified from pTRE-TIGHT miR-1 (Addgene plasmid 14896) (Lewis et al., 2003), generating SphI and SbfI restriction sites on the 5′end. This fragment was cloned into pUAS-tdT via SphI/EcoRI restriction sites, replacing the UAS-hsp70 sequence and giving pTRE-tdT. The same fragment was digested with SbfI/EcoRI and cloned into the corresponding sites in pUAS-luc2, replacing the UAS-hsp70 sequence and giving pTRE-luc2.

plexAop2-luc2

lexAop2-hsp70 minimal promoter was amplified from pJFRC18-8XLexAop2-mCD8::GFP (Addgene plasmid 26225) (Pfeiffer et al., 2010), generating the EcoRI restriction site on the 3′ end. The PCR fragment was digested with SbfI/EcoRI and cloned into the corresponding sites in pUAS-luc2, replacing UAS-hsp70 sequence and giving pLexAop2-luc2.

pUAS-Cre

Cre recombinase was amplified from pNrl-Cre (Addgene plasmid 13780) (Matsuda and Cepko, 2007), generating an EcoRI-Kozak sequence and XbaI restriction site on the 5′ and 3′ ends, respectively. This fragment was inserted in place of luc2 in the pUAS-luc2 vector via EcoRI/XbaI restriction sites.

p10xUAS-ChR2-mCherry

ChR2/H134R-mCherry amplicon was flanked with EcoRI/XbaI on the 5′ and 3′ ends, respectively, and inserted into a 10xUAS vector via EcoRI/XbaI sites.

pCAG-N-Gal4DBD

The Gal4 DNA-binding domain (Gal4DBD) was amplified from pAcPL-Gal4DBD (Addgene plasmid 15304) (Luan et al., 2006), with AgeI-Kozak consensus sequence and NheI-10Glycine-MfeI-NotI overhangs on the 5′ and 3′ ends, respectively. This fragment was inserted in place of EGFP in the pCAG-GFP vector via AgeI/NotI restriction sites.

pCAG-C-Gal4DBD

The GAL4 DNA-binding domain (Gal4DBD) was amplified from pAcPL-Gal4DBD (Addgene plasmid 15304) (Luan et al., 2006), with AgeI-NheI and NotI overhangs added on the 5′ and 3′ ends, respectively. This fragment was inserted in place of EGFP in the pCAG-GFP vector via AgeI/NotI restriction sites.

pCAG-VP16AD

The VP16 activation domain (VP16AD), along with a NheI-10Glycine polylinker on the 3′ end, was amplified from pAcPL-VP16 (Addgene plasmid 15305) (Luan et al., 2006), generating AgeI-Kozak consensus sequence and NotI restriction site on the 5′ and 3′ ends, respectively. This fragment was inserted in place of EGFP in the pCAG-GFP vector via AgeI/NotI restriction sites.

GBP1+6 T-DDOG Constructs

GBP1-Containing Plasmids

In all GBP1-containing constructs, GBP1 was amplified from pUC57-GBP1 with primers bearing various overhangs on the PCR products.

pCAG-GBP1-10 gly-Gal4DBD. AgeI-Kozak-GBP1-NheI PCR fragment was cloned into pCAG-C-Gal4DBD via AgeI/NheI sites.

pCAG-Gal4DBD-10 gly-GBP1. NheI-10 gly-MfeI-GBP1-NotI PCR fragment was cloned into pCAG-N-Gal4DBD via NheI/NotI sites.

pCAG-Gal4DBD-GBP1. NheI-GBP1-NotI PCR fragment was cloned into pCAG-N-Gal4DBD via NheI/NotI sites.

pCAG-Gal4DBD-GBP1x2. NheI-GBP1-NheI PCR fragment was cloned into pCAG-Gal4DBD-10 gly-GBP1 via NheI restriction site.

pCAG-VP16AD-10 gly-GBP1. NheI-10 gly-MfeI-GBP1-NotI PCR fragment was cloned into pCAG-VP16AD via NheI/NotI sites.

pCAG-rTetRDBD-GBP1. The DNA-binding domain of Reverse Tetracycline transactivator 3G (rtTA3G) was amplified from pLenti CMV rtTA3G Blast (R980-M38-658) (Addgene plasmid 31797, Dominic Esposito). The PCR product contains AgeI-Kozak consensus sequence and NheI restriction site on the 5′ and 3′ ends, respectively. This fragment was cloned into pCAG-Gal4DBD-GBP1 via AgeI/NheI and replaces Gal4DBD.

pCAG-GBP1-10 gly-lexADBD. The LexA DNA-binding domain (LexA DBD) was amplified from pCMV Lex VP16 HA (P#1708) (Addgene plasmid 14593) (Kurosu and Peterlin, 2004) with NheI-10 gly-XbaI and NotI overhangs on the 5′ and 3′ ends, respectively. This fragment was cloned into pCAG-GBP1-10 gly-Gal4DBD via NheI/NotI and replaces Gal4DBD.

GBP6-Containing Plasmids

For all GBP6-containing constructs, GBP6 was amplified from pUC57-GBP6 with various overhangs on the PCR products.

pCAG-Gal4DBD-GBP6. NheI-GBP6-NotI PCR product was cloned into pCAG-N-Gal4DBD via NheI/NotI restriction sites.

pCAG-VP16AD-GBP6. NheI-GBP6-NotI PCR product was cloned into pCAG-VP16AD via NheI/NotI restriction sites

pCAG-GBP6-10 gly-Gal4DBD. AgeI-Kozak consensus-GBP6-NheI was cloned into pCAG-C-Gal4DBD via AgeI/NheI sites.

pCAG-GBP6-10 gly-VPminx2, pCAG-GBP6-10 gly-VPminx3, pCAG-GBP6-10 gly-VPminx4. The VPminx2, x3, x4 sequences were amplified from CMV rtTA3G Blast (R980-M38-658) (Addgene plasmid 31797, Dominic Esposito) with NheI-10 gly-MfeI and NotI overhangs on the 5′ and 3′ end, respectively. Each PCR fragment was separately cloned into pCAG-GBP6-10 gly-Gal4DBD.

pCAG-p65AD-GBP6. The p65 activation domain (p65AD) was amplified from pCMV4 p65 (Addgene plasmid 21966) (Ballard et al., 1992) with the NLS from SV40 large T-antigen. This fragment was amplified again to add AgeI-Kozak consensus sequence and NheI on the 5′ and 3′ end, respectively. The final PCR product was cloned into pCAG-VP16AD-GBP6 via AgeI/NheI, replacing VP16AD.

IRES-Linked, GBP1+6 T-DDOG Constructs

pCS2+-Gal4DBD-GBP1-IRES-p65AD-GBP6. Gal4DBD–GBP1 and p65AD-GBP6 were linked with an IRES by SOE PCR, adding BamHI/EcoRI on the 5′ and 3′ ends, respectively. This fusion PCR product was cloned into pCS2+ via BamHI/EcoRI sites.

GBP2+7 T-DDOG Constructs

pCAG-GBP2-10 gly-Gal4DBD. GBP2 was amplified from GBP2 chromobody plasmid with AgeI-Kozak and NheI sequences on the 5′ and 3′ ends, respectively. This fragment was cloned into pCAG-C-Gal4DBD via AgeI/NheI sites.

pCAG-VP16AD-10 gly-GBP7. GBP7 was amplified from GBP7 chromobody plasmid with NheI-10 gly-MfeI on the 5′ end and NotI on the 3′ end. This fragment was cloned into pCAG-VP16AD via NheI/NotI sites.

pCAG-Gal4DBD-GBP2. GBP2 was amplified from GBP2 chromobody plasmid with NheI and NotI sequences on the 5′ and 3′ ends, respectively. The PCR product was cloned into pCAG-N-Gal4DBD via NheI/NotI restriction sites.

pCAG-GBP7-p65AD. GBP7 was amplified from pCAG-p65AD-10 gly-GBP7, adding AgeI-Kozak-NLS and MfeI sequences on the 5′ and 3′ ends, respectively. The PCR product was cloned into pCAG-GBP7-10 gly-p65AD via AgeI/MfeI, replacing NLS-less GBP7 and a 10 glycine linker.

GBP1+5 T-DDOG Constructs

pCAG-GBP5-10 gly-Gal4DBD. GBP5 was amplified from GBP5 chromobody plasmid with AgeI-Kozak consensus sequences and NheI on the 5′ and 3′ end, respectively. The final PCR product was inserted into pCAG-C-Gal4DBD via AgeI/NheI, replacing GBP1.

pCAG-GBP1-10 gly-VPminx2. VPminx2 sequences were amplified from CMV rtTA3G Blast (R980-M38-658) (Addgene plasmid 31797, Dominic Esposito) with NheI-10 gly-MfeI and NotI overhangs on the 5′ and 3′ end, respectively. The PCR fragment was cloned into pCAG-GBP1-10 gly-Gal4DBD via NheI/NotI, replacing 10 gly-Gal4DBD.

Cell Culture and Transfection

Unless stated otherwise, for all cell culture experiments, 1-2x10^5 293T cells were seeded into 48 well plates and 1-2 days later transfected with plasmids. Plasmids were transfected via polyethyleneimine (PEI) at a 1:4 DNA amount:PEI volume ratio. For doxycycline-inducible experiments, doxycycline hyclate (Sigma, D9891-10G) was diluted in water and used at concentrations up to 1 μg/ml.

Cell Culture tdT Reporter Readout

A total of 500 ng of DNA were transfected. In all experiments, 100 ng of UAS-tdT or TRE-tdT were included. Plasmids encoding CAG-driven XFP, DBDG, ADG and other variants were transfected at amounts adjusted for their molarity. pBS SK+, pCAGEN, or

pCAG-mCherry were added to adjust the total DNA amount to equal levels. Fluorescent micrographs were taken on a Leica DMI3000B microscope with a 10x or 20x objective.

Luciferase Assay

In all experiments, 12.5 ng pUAS-luc2 and 1.25 ng pRL-TK were included. Plasmids encoding CAG-driven XFP, DBDG, ADG and other variants were transfected at amounts adjusted for their molarity. pBS SK+ or pCAGEN was added to adjust the total DNA amount to 62.5 or 63.5 ng. Cells were harvested 24 hr later for dual-luciferase assay (Promega) according to manufacturer's instructions. Lysates were pipetted into 96-well plates and read in an Analyst GT plate reader (Molecular Devices). To determine the linear range of detection for the plate reader, a standard curve was constructed by measuring luciferase activity of serial dilutions of QuantiLum recombinant luciferase (Promega). Transfection amounts were then optimized to give readings within the linear range of detection for the instrument. Comparisons between experimental conditions were only done when cell lysates were assayed at the same time. All transfection conditions were repeated 2 or 3 times. Cell lysate from each repeat was split into 3 samples for luciferase assay. 2-tailed Student t test assuming unequal variance was used to test for significance, judged to be $p < 0.05$.

Dosage Response Curve Experiment

A total of 100 ng total DNA were transfected. 15.5 ng of pCAG-Gal4DBD-GBP6 and pCAG-VP16-10lk-GBP1, 12.5 ng pUAS-luc2 and 1.25 ng pRL-TK were included. CAG-GFP plasmid was serially diluted 3 fold in water and pipetted at equal volume into transfection mixture. pCAG-mCherry plasmid was used to make up the total DNA amount. 24 hr after transfection, cells were imaged on Leica epifluorescence microscope at 20x for GFP and mCherry fluorescence before being used for dual-luciferase assay (Promega). All transfection conditions were repeated 3 times. Cell lysate from each repeat was split into 3 samples for luciferase assay.

General Microscopy and Image Analysis

Retinal sections or whole-mount retinas were taken on a Zeiss LSM780 confocal microscope. Slides were scanned using a 40x or 63x oil immersion objective. Cell culture and zebrafish images were images were obtained on a Leica DMI3000B epifluorescence microscope. Whenever possible, image settings were adjusted for saturation. Whenever samples were to be compared within an experiment, image settings and processing were kept constant. Images were analyzed and processed on Imaris, Image J and/or Photoshop software. Images from in vivo electroporation were smoothened on Imaris using the median filter as 3x3x1pixel dimension. Image contrast was adjusted either in Imaris and/or Photoshop.

Retinal Histology

Mouse retinas were dissected out of the eyes or harvested from culture and fixed at room temperature for 30 min in 4% paraformaldehyde. Fixed retinas were washed in PBS and equilibrated in increasing concentration of sucrose (10/30%) 1xPBS pH 7.4 solutions. Retinas were then equilibrated in OCT for at least 10 min and quickly frozen on dry ice. Retinal cryosections were cut into 20 or 25 μm slices on a Leica CM3050S cryostat (Leica Microsystems), using disposable blades.

Retinal Immunohistochemistry

Retinal cryosections were blocked in 5% heat-inactivated normal goat serum in 0.1% TritonX-1xPBS (PBT), pH7.4 for 1 hr at room temperature and then stained with primary antibody in blocking solution overnight at 4°C. Slides were washed in 1xPBT for three times and then incubated in secondary antibodies and DAPI (0.3 μM) for 2 hr at room temperature. Slides were then washed in 1xPBT for three times and mounted using Fluormount-G (Southern Biotechnology Associates; 0100-01).

Antibodies

Antibodies used in this study were: chicken anti-β-galactosidase (1:1000 dilution) (ab9361, Abcam), rabbit anti-OTX2 (1:500 dilution) (AB9566, Chemicon), mouse anti-PAX6 (1:20 dilution) (Pax6 s, Developmental Studies Hybridoma Bank), goat anti-ChAT (1:100 dilution for retinal section, 1:200 dilution for wholemount retina) (AB144, Millipore), rabbit anti-GFP (1:500 dilution) (A-6455, Invitrogen) or chicken anti-GFP (1:1000 dilution) (ab13970) were only used on Tg(GUS8.4-GFP) and mGluR6-GFP to amplify the weak native GFP signal and reveal axonal processes, Rabbit anti-dsRed (1:1000 dilution) (632496, Clontech), Rabbit anti-Calbindin D-28k (1:2000 dilution) (CB38a, Swant), Mouse anti-Calretinin (1:2000 dilution) (MAB 1568, Millipore).

Secondary antibodies raised against the relevant species were obtained from Jackson ImmunoResearch or Invitrogen.

Additional Information for Retinal In Vivo Experiments and Analyses

In Vivo Retinal Electroporation

Postnatal day 0 to 5 (P0-P5) mouse pups were electroporated in vivo as described previously (Matsuda and Cepko, 2004), except that a Femtojet Express pressure injector (Eppendorf;920010521) delivered the DNA via a custom made glass needle (Origio, C060609). DNA solutions (1-1.5 μg/μl) were injected through the sclera and into the subretinal space of the mouse retina. pCAGEN served as an empty vector substitute for excluded plasmids. For demonstration of GFP as a spatial regulator of gene expression in CD1 retinas, GFP, DBDG, and ADG plasmids were electroporated at following DNA mass ratios: CAG-GFP:DBDG:ADG – 3:2.5:1,

Rho-GFP:DBDG:ADG - 3:2.5:1.25, mGluR6-GFP:DBDG:ADG - 4:2.5:1.25. For Tg(GUS8.4GFP) experiment, DBDG:ADG DNA mass ratio was kept at 2.5:1 DNA mass ratio.

Quantification of Electroporated Retinas

20 μm thick retinal cryosections were immunostained for chicken anti-βgal and imaged via confocal microscopy. Regions of dense electroporation were selected for quantification. Quantifications were done on ImageJ using the Cell Counter plugin. The Imaris program aided analyses. To begin, cells expressing a given marker were randomly chosen throughout the confocal stack. Selected cells were then analyzed for co-expression with additional genes, represented by co-localization of fluorescent signals emitted by the chosen channels. A gene was judged, by eye, to be expressed in a cell if its corresponding fluorescent signal was enriched within the selected cell body relative to the surrounding. Individual slices of a confocal stack were analyzed for this purpose. We detected very little n-βgal in the INL even when GFP and tdT were strongly expressed in the layer. This is likely due to a combination of poor expression and/or poor antibody detection. Thus, we limited our analyses n-βgal+ marked cells in the ONL. To sample the mean of each retina, at least 50 and 20 cells were quantified for each marker type in the ONL and INL, respectively. The mean of each parameter was averaged across retinas and plotted as mean ± SEM.

The coelectroporation efficiency between two plasmids was estimated by measuring the percentage of CAG-GFP+ cells per n-βgal+ (from CAG-nlacZ expression) cell in the ONL. This was found to be 91 ± 2% (mean ± SD) (n = 3 retinas). Thus, the probability that 4 plasmids will be electroporated into a cell is approximately $0.91^3 = 0.75$. We divided the non-adjusted efficiency of tdT activation (quantified in bottom of Table S6) by this probability (in percentage). This produces the adjusted efficiency of the T-DDOG system.

In retinas strongly electroporated with DNA including mGluR6-GFP and Gal4-GBP1$^{p65\text{-}GBP6}$, some leakage of mGluR6 promoter was detected in the ONL, giving weak GFP fluorescence. Leakage from mGluR6 promoter was likely, since a mGluR6-ERT2-CreERT2 construct also activated floxed reporter expression in the ONL under similar electroporation conditions. However, leaky GFP was not detected when mGluR6-GFP was electroporated without Gal4-GBP1$^{p65\text{-}GBP6}$ components, even after GFP antibody staining. The appearance of leaky ONL GFP may thus be due to a combination of the fluorescence enhancing ability of GBP1 (Kirchhofer et al., 2010) and/or slight GFP stabilization by T-DDOG components. By immunostaining GFP with a polyclonal GFP antibody, and imaging the antibody signal at wavelengths distinct from the GFP emission range, we detected stabilized GFP expression only in the presence of Gal4-GBP1$^{p65\text{-}GBP6}$ but not Gal4-GBP2$^{p65\text{-}GBP7}$. This suggests that Gal4-GBP1$^{p65\text{-}GBP6}$, but not Gal4-GBP2$^{p65\text{-}GBP7}$, can have some stabilizing effect on GFP. Nevertheless, the leaky GFP fluorescence was barely above background and induced little to no UAS-tdT expression. Due to the difficulty distinguishing the weak GFP signals from background noise, it was difficult to quantify the distribution of GFP/tdT expressing cells in the ONL cell count. We thus chose to represent the enrichment of tdT/GFP expression in the INL relative to the ONL by comparing the fluorescent intensity of the fluorescent proteins in the ONL and INL. Owing to the low background in tdT fluorescent channels, we were able to identify weak tdT+ cells in the ONL with better confidence, so we randomly chose tdT+ cells from both the ONL and INL, quantified fluorescent intensity within cell bodies in single confocal stacks, and measured the corresponding GFP signal within the selected cell bodies. Arbitrary units were obtained as in OTX2 quantification analysis, with the background control being obtained directly next to the chosen cell body.

ON/OFF Bipolar Cell Identification

ON/OFF bipolar cells were distinguished by their axonal stratification in the inner plexiform layer (IPL), following criteria described previously (Ghosh et al., 2004). 20 μm thick retinal sections were stained for rabbit anti-GFP and goat-anti-ChAT, followed by confocal imaging. Confocal stacks of retinal sections were used for analysis. Electroporated GFP+ or GFP+/tdT+ bipolar cells were traced along their axonal processes to the IPL, where the identification of ON/OFF cell was based on the processes' location relative to cholinergic bands labeled by anti-ChAT. ON bipolar processes were those that fell below the midline between the two cholinergic bands (Ghosh et al., 2004).

Otx2 Removal Experiment

Ex Vivo Retinal Electroporation

P0 *Otx2*$^{fl/fl}$ (Tian et al., 2002) were electroporated ex vivo with pCAG-GBP1-10 gly-Gal4DBD (100ng/μl), pCAG-p65AD-GBP6 (50ng/μl), pUAS-Cre (40ng/μl), pCAG-nlacZ (100ng/μl). pCAG-GFP (100ng/μl) or pCAG-dsRed (100ng/μl) was used depending on the experimental conditions. Ex vivo electroporation was carried out as described (Emerson and Cepko, 2011) except that retinas were cultured ex vivo for 8 days before harvesting.

Otx2 Expression Quantification

Electroporated cells labeled by either GFP, dsRed, and/or n-βgal were quantified for OTX2 antibody staining. Using ImageJ, a mask for the chosen cell body was created on the GFP, dsRed, or n-βgal channel and transferred to the OTX2 immunofluorescence channel. Measurements of the mean pixel intensity on single confocal slices were taken for the chosen cell bodies. Each measurement was paired with a background fluorescence intensity measurement from the same slice, chosen at a location in the slice where no cells were present. Although the best background control is one taken right next to the cell, we were unable to do this because OTX2 staining is quite widespread and we could not tell whether faint staining signals on the retina slice were real or not. Our choice of background thus gives the impression that OTX2 is still present at a low level above background, but in fact the real baseline level is above 0. Each measurement was then subtracted from the background to obtain the net fluorescence. As a control,

non-electroporated cells, as determined by a lack of GFP, dsRed or n-βgal expression, were also measured for OTX2 immunostaining level. 20 measurement pairs were made for each set of condition per retina. Measurements were normalized by dividing the intensity values from each electroporated or non-electroporated cell by the average intensity of the non-electroporated cells from the same confocal stack. Values were then multiplied by 100 to obtain the arbitrary unit (a.u.). The average OTX2 immunostaining fluorescence intensity was plotted as a histogram binned at 10 a.u. per bar. 2-tailed Student t test assuming unequal variance was used to test for significance, judged to be $p < 0.05$.

PAX6 ONL Quantification

Confocal images were used to quantify number of PAX6 immunopositive cells in the ONL of electroporated and non-electroporated retinal patches. Electroporated retinal patches were identified by the presence of GFP or dsRed expression, and non-electroporated retinal patches were identified by the absence of GFP or dsRed expression. Quantification were performed over 12 slices of confocal images at an interval of 1 μm/slice. A total of 10 confocal stacks taken from 5 retinas were analyzed per condition. For each retina, two confocal stacks were taken from two different regions separated by at least 200 μm. The identification of ONL was aided by DAPI staining. Counting of PAX6-positive cells in the ONL was aided by the cell counter plugin in ImageJ. Results are presented as a boxplot which depicts the median as the central bar in the box, and the maximum and minimum values as the whiskers. To test for statistical significance, 2-tailed Student t test was performed, assuming unequal variance. Statistical significance occurs when $p < 0.05$.

Brain Recordings and Structural Analyses

In Utero Electroporation

Embryonic day (E)15.5 timed-pregnant female C57BL/6 mice were deeply anesthetized with 2% isoflurane. Uterine horns were exposed and periodically rinsed with warm PBS. Plasmids (1-1.5 μg/μl) were injected into the lateral ventricle of one cerebral hemisphere. Five voltage pulses (50 V, 50 ms duration, 1 Hz) were delivered with round plate electrodes (CUY21 electroporator, NEPA GENE, Japan). Injected embryos were placed back and allowed to mature to delivery.

Slice Preparation

Acute brain slices were obtained from electroporated mice (P8-14) using standard procedures. Mice were deeply anesthetised with isoflurane. The brain was quickly removed and placed into chilled choline-based cutting solution containing (in mM) NaHCO3 (25), NaH2PO4 (1.25), KCl (2.5), MgCl2 (7), glucose (25), CaCl2 (1), choline chloride (110), ascorbic acid (11.6), and pyruvic acid (3.1). The brain was cut coronally at 300μm thickness using a Leica VT1000S vibratome (Leica Instruments, Nussloch, Germany). Slices were placed in a glass chamber filled with artificial cerebrospinal fluid (ACSF) containing (in mM) NaCl (127), KCl (2.5), NaHCO3 (25), NaH2PO4 (1.25), CaCl2 (2), MgCl2 (1) and glucose (25). Cutting and ACSF solutions were saturated with 95% O_2 and 5% CO_2. Slices were incubated at 34°C for 30 min before the experiments.

Electrophysiology

Individual slices were transferred to a recording chamber mounted on an upright microscope (Olympus BX51WI) and continuously superfused (2–3 ml/min) with artificial cerebrospinal fluid at room temperature. Cells were visualized through a 60X water-immersion objective with either infrared differential interference contrast optics or epifluorescence to identify GFP^-/tdT^+, GFP^+/tdT^-, and GFP^+/tdT^+ neurons. Whole-cell current clamp recordings were obtained from cortical layer 2/3 pyramidal neurons in the region of dense electroporation at P8-12. Patch pipettes (2.5–3.5 MΩ) pulled from borosilicate glass (G150F-3, Warner Instruments) were filled a K+ based internal solution, composed of 135 mM KMeSO4, 5 mM KCL, 5 mM HEPES, 4 mM MgATP, 0.3 mM NaGTP, 10 mM Na2-CrePO4 (pH 7.4). Hyperpolarizing and depolarizing 1,000 ms-long step currents were injected to measure the input resistance, membrane time constant, and action potential responses of each cell.

Two-Photon Imaging

Two-photon laser-scanning microscopy (2PLSM) was performed using a custom microscope as previously described (Carter and Sabatini, 2004). Cell morphology was visualized at P12-14 using Alexa Fluor 594 (10–20 μM) excited with 810 nm light and introduced into the cell through whole-cell recording. A 2PLSM 3-dimensional image stack through each neuron was collected, followed by stacks through 2-3° dendritic segments at a 10-fold higher magnification. For dendritic spine density and spine shape analyses, cells were analyzed used custom-written routines in MATLAB. The size of each spine was measured in the optical section of maximal brightness and dendritic length was estimated from Z projections.

Data Acquisition and Analysis

Membrane voltage deflections were amplified and low-pass filtered at 3 kHz using a Multiclamp 700B amplifier (Molecular Devices), digitized at 10 kHz and acquired using National Instruments acquisition boards and a custom version of ScanImage written in MATLAB (Mathworks) (Pologruto et al., 2003). Electrophysiology and imaging data were analyzed offline using Igor Pro (Wavemetrics) and ImageJ (NIH). In figures, current-clamp traces represent a single acquisition. Data (reported as mean ± SEM) were compared statistically using one-way ANOVA. $p < 0.05$ were considered statistically significant.

Fixed-Tissue Preparation and Imaging

Mice were transcardially perfused with 4% paraformaldehyde and brains were post-fixed for 2 days. Brains were sectioned coronally at 60μm using a Vibratome. No immunoenhancement was used to increase the signal of native fluorophores. Images were acquired with an Olympus VS110 microscope and Olympus FV1000 laser scanning confocal microscope (Harvard Neurobiology Imaging Facility).

Optogenetic Recordings of Mouse Retina

Electroporation

Electroporation was done as stated in the in *vivo* electroporation section. In addition to the T-DDOG components and 10xUAS-ChR2-mCherry, we introduced 5xUAS-tdT in order to boost the fluorescence signal in the retina. This was done to aid the identification of electroporated patches for recordings. CAG-nlacZ was also included as an electroporation marker.

Preparation of Retinas

Retina isolation was done under red illumination (peak wavelength at 580 nm) in Ringer's medium (110 mM NaCl, 2.5 mM KCl, 1 mM $CaCl_2$, 1.6 mM $MgCl_2$, 10 mM D-glucose, 22 mM $NaHCO_3$, bubbled with 5% CO_2/95% O_2, pH 7.4). The retinas were then mounted ganglion cell-side up on filter paper (Millipore, MA) that had a 4-5 mm diameter rectangular aperture in the center, and superfused in Ringer's medium at 35–36°C in the microscope chamber for the duration of the experiment.

Targeting Cells in Wholemount

We visualized red and green fluorescent bipolar cells by using a custom made 2-photon microscope equipped with a Mai Tai HP two-photon laser (Spectra Physics) tuned to 920 nm. Infrared illumination allowed the visualization of the retina with a CCD camera (Diagnostic Instruments) during two-photon scanning. GCL cells, which had fluorescent bipolar cells in their dendritic field were targeted by patch electrodes. A small area above the GCL cells was cleaned from Müller cell end feet using infrared imaging with a patch pipette filled with mouse Ringer's solution. Then the patch electrode was moved into close proximity of the targeted cell and loose cell-attached mode was established. (http://www.youtube.com/watch?v=Epfpnh1jxaU).

Electrophysiology and Pharmacology

Electrophysiological spike recordings were made using an Axon Multiclamp 700B amplifier (Molecular Devices) and borosilicate glass electrodes (Sutter Instrument). Signals were digitized at 10 kHz (National Instruments) and acquired using custom software written in LabVIEW (National Instruments). Data were analyzed offline using MATLAB (MathWorks). The spiking responses were recorded using the patch clamp technique in loose cell-attached mode with electrodes pulled to between three and five MΩ resistance and filled with Ringer's medium. In order to visualize GCL cells in some experiments after spike recordings, neurobiotin (Vector Laboratories) and Alexa 488 (Molecular Probes) were delivered using patch pipette, pulled to between five and eight MΩ resistance and filled with 112.5 mM $CsCH_3SO_3$, 1 mM $MgSO_4$, 7.8×10^{-3} mM $CaCl_2$, 0.5 mM BAPTA, 10 mM HEPES, 4 mM ATP-Na_2, 0.5 mM GTP-Na_3, 5 mM lidocaine N-ethyl bromide (QX314-Br), 7.5 mM neurobiotin chloride, 13 mM Alexa 488. The pH was adjusted to 7.2 with CsOH. In pharmacological experiments, 20 μM APB (L-(+)-2-amino-4-phosphonobutyric acid, blocking metabotropic glutamate receptors) (Calbiochem) was bath-applied.

Light Stimulation

Photoreceptors and were stimulated with light generated by a digital light processor (DLP) projector at 75 Hz (V-339 PLUS Vision Corp.). The same DLP projector provided the infrared light for patch clamp recordings. The maximum power produced by the projector was 229 ± 35 mW/cm^2 (mean ± SEM). We measured light projected through the objective lens at the focal plane on the stage. Light intensity was measured with a photodiode power meter (in Watts per cm^2; Model S130VC; Thorlabs), and the spectrum was measured with a spectrometer (Model USB4000-UV-VIS; Ocean Optics). We have expressed light intensity in number of photoisomerizations per rod per second (R*/s). The light path was computer-controlled with a shutter (SC10, Thorlabs). Light intensity was modulated by neutral density filters, which were built into two filter wheels (FW102, Thorlabs).

For photoreceptor stimulation, the light was focused on the outer segments of photoreceptors in the wholemount retina. For photoreceptor stimulation the light intensity was 1.3×10^3 R*/s. The contrast for photoreceptor stimulation was 2000. For ChR2 stimulation the light was focused on the bipolar cell layer. ChR2/H134R was activated with a 2 s light flash at ~10^8 R*/s generated by a 120 W mercury epifluorescent lamp (X-Cite 120 PC, Lumen Dynamics). The stimulus was generated using software written in LabVIEW (National Instruments) and Python.

Postrecording Immunohistochemistry

For whole-mount immunohistochemistry, fixed retinas were freeze/thawed at least 3 times in 30% sucrose/PBS solution. Retinas were then blocked in 10% normal donkey serum, 1% BSA and 0.35% PBT. Antibody stainings were done in 3% normal donkey serum, 1% BSA, and 0.4% PBT. Primary antibody incubations were done at room temperature for 3-4 days. Retinas were washed with PBS, treated with secondary antibody and washed again with PBS. Retinas were then stained for neurobiotin using streptavidin-Alexa 649 probes in 0.5% PBT overnight at room temperature. Washed retinas were flat-mounted and imaged with confocal microscopy. Antibody stainings were done for anti-ChAT to analyze stratification and anti-dsRed to boost mCherry/tdT signals.

Screens

T-DDOG Screen

A total of 6 GBPs (GBP1, 2, 4, 5, 6, and 7) were used for all T-DDOG screens. Each GBP was fused to a DBD or an AD at either its N- or C-terminal end. Fusions were made with either no linker between the two protein modules, or with a 10 amino acid glycine linker. Most chimeric constructs carried a nuclear localization signal (NLS) at the N-terminal end. All chimeric constructs were placed under the control of the ubiquitous CAG promoter. The resulting CAG-chimera plasmids were combined in many possible pairwise combinations and transfected along with pCAG-GFP, UAS-luc2 and pRL-TK into 293T cells. Combinations that gave the strongest reporter induction after 24 hr were selected for further characterization.

rTetR-based T-DDOGs were screened similarly as above, but transfection mixtures for each DBDG:ADG combination was split into two culture wells, one with 1 μg/ml doxycycline and the other with no doxycycline. Functional combinations were judged to be those that gave strong reporter induction in the presence of doxycycline, but not in the absence of doxycycline.

Rod Mispositioning Screen

In our initial attempts to apply Gal4-GBPX$^{VP16\text{-}GBPY}$ in the retina, we observed that T-DDOGs with VP16AD induced mispositioning of rod photoreceptors in the upper (sclera) half of the ONL. This phenotype was seen in retinas electroporated with VP16AD-GBPX, but not with Gal4DBD-GBPX plasmids. The phenotype also was independent of UAS-transgene activation or Gal4-GBPX$^{VP16\text{-}GBPY}$ interaction with GFP, since we observed the same phenotype in electroporated cells not expressing GFP and UAS-tdT, but expressing Gal4-GBPX$^{VP16\text{-}GBPY}$. Thus, high levels of VP16AD likely played a major role in the mispositioning of rod photoreceptors. The mechanism behind this is likely due to squelching effect of potent activation domains (Gill and Ptashne, 1988).

To overcome this problem, we screened for ADs that did not give the mispositioning phenotype. The most useful ADs would be those that confer high transcriptional activity with minimal side effects on cellular phenotype. To determine the best AD for use in the retina, selected T-DDOGs involving p65 or VPmin ADs were electroporated into P0 CD1 retina along with CAG-GFP, UAS-tdT and CAG-nlacZ. We chose from T-DDOGs that gave strong GFP-dependent induction of UAS-luc2 in 293T cells. Electroporation mixtures including VP16AD served as the positive control for the rod phenotype, while those missing DBDG and ADG plasmids served as the negative control. DNA mass amount was kept constant for all conditions, with GFP:DBDG:ADG plasmid ratio at 2:2:1.

Of the 13 T-DDOGs tested, those utilizing p65 as the AD consistently gave the most normal positioning of rod photoreceptors. T-DDOGs utilizing VPminx2 also had reduced mispositioning phenotype, but their activities were also relatively weaker than that of p65. T-DDOGs utilizing VPminx3 or x4 strongly induced UAS-tdT activity, but they also caused obvious photoreceptor mispositioning. Given these results, we chose to work with p65AD in our in vivo/ex vivo experiments. It should be noted that whether a particular AD will cause abnormality in the host cell depends largely on the context, such as cell type identity, method of T-DDOG delivery, expression level of T-DDOG components, etc. This is well documented in other gene regulatory systems using transcription factors (Asakawa et al., 2008; Kramer and Staveley, 2003; Morimoto and Kopan, 2009; Pfeiffer et al., 2010; Potter et al., 2010). For example, we found that electroporation of high amounts of p65AD plasmids in similar DNA mixtures eventually led to rod mispositioning. Thus, we stress the importance of always performing proper controls to rule out potential side effects caused by overexpression of AD.

SUPPLEMENTAL REFERENCES

Asakawa, K., Suster, M.L., Mizusawa, K., Nagayoshi, S., Kotani, T., Urasaki, A., Kishimoto, Y., Hibi, M., and Kawakami, K. (2008). Genetic dissection of neural circuits by Tol2 transposon-mediated Gal4 gene and enhancer trapping in zebrafish. Proc. Natl. Acad. Sci. USA *105*, 1255–1260.

Ballard, D.W., Dixon, E.P., Peffer, N.J., Bogerd, H., Doerre, S., Stein, B., and Greene, W.C. (1992). The 65-kDa subunit of human NF-kappa B functions as a potent transcriptional activator and a target for v-Rel-mediated repression. Proc. Natl. Acad. Sci. USA *89*, 1875–1879.

Carter, A.G., and Sabatini, B.L. (2004). State-dependent calcium signaling in dendritic spines of striatal medium spiny neurons. Neuron *44*, 483–493.

Emerson, M.M., and Cepko, C.L. (2011). Identification of a retina-specific Otx2 enhancer element active in immature developing photoreceptors. Dev. Biol. *360*, 241–255.

Huang, L., Shanker, Y.G., Dubauskaite, J., Zheng, J.Z., Yan, W., Rosenzweig, S., Spielman, A.I., Max, M., and Margolskee, R.F. (1999). Ggamma13 colocalizes with gustducin in taste receptor cells and mediates IP3 responses to bitter denatonium. Nat. Neurosci. *2*, 1055–1062.

Kramer, J.M., and Staveley, B.E. (2003). GAL4 causes developmental defects and apoptosis when expressed in the developing eye of *Drosophila melanogaster*. Genet. Mol. Res. *2*, 43–47.

Kurosu, T., and Peterlin, B.M. (2004). VP16 and ubiquitin; binding of P-TEFb via its activation domain and ubiquitin facilitates elongation of transcription of target genes. Curr. Biol. *14*, 1112–1116.

Lewis, B.P., Shih, I.H., Jones-Rhoades, M.W., Bartel, D.P., and Burge, C.B. (2003). Prediction of mammalian microRNA targets. Cell *115*, 787–798.

Morimoto, M., and Kopan, R. (2009). rtTA toxicity limits the usefulness of the SP-C-rtTA transgenic mouse. Dev. Biol. *325*, 171–178.

Pfeiffer, B.D., Ngo, T.T., Hibbard, K.L., Murphy, C., Jenett, A., Truman, J.W., and Rubin, G.M. (2010). Refinement of tools for targeted gene expression in Drosophila. Genetics *186*, 735–755.

Pologruto, T.A., Sabatini, B.L., and Svoboda, K. (2003). ScanImage: flexible software for operating laser scanning microscopes. Biomed. Eng. Online *2*, 13.

Potter, C.J., Tasic, B., Russler, E.V., Liang, L., and Luo, L. (2010). The Q system: a repressible binary system for transgene expression, lineage tracing, and mosaic analysis. Cell *141*, 536–548.

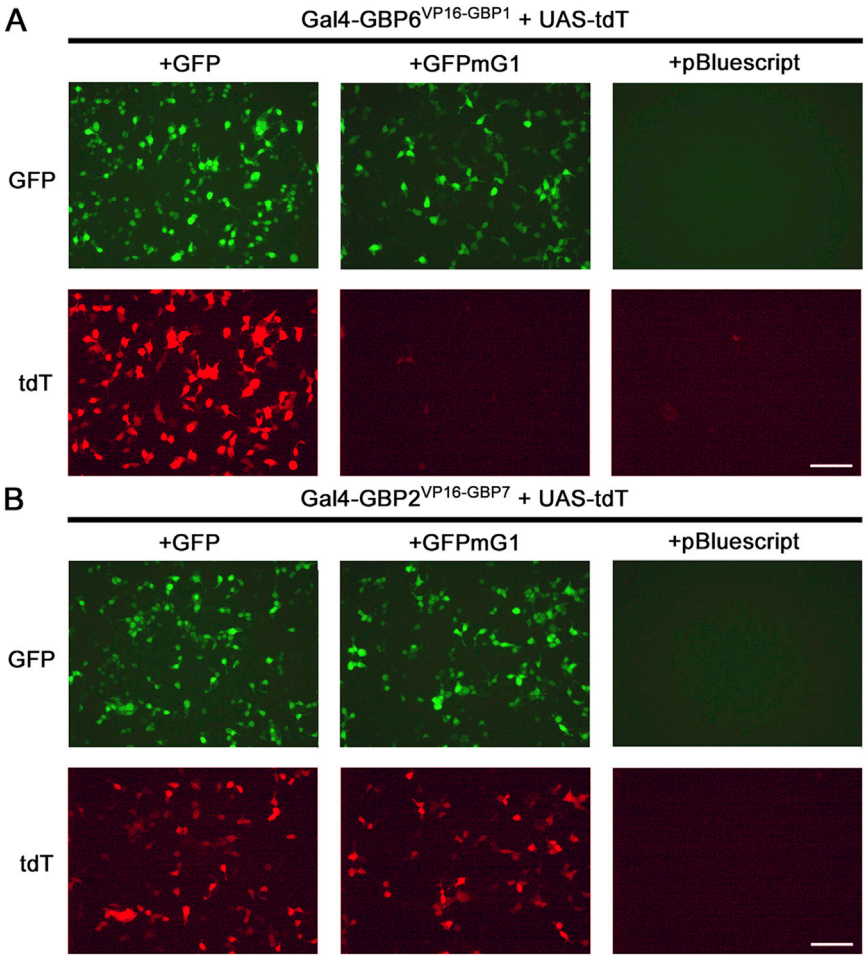

Figure S1. GFP-Dependent Activation of UAS-tdT In Vitro, Related to Figure 2

(A and B) Representative images of Gal4-GBP6$^{VP16\text{-}GBP1}$ (A) and Gal4-GBP2$^{VP16\text{-}GBP7}$ (B) activation of an UAS-tdT reporter in 293T cells. Cells were transfected with all indicated constructs and imaged 16 hr post-transfection. GFP, GFPmG1, DBDG and ADG constructs were delivered in separate plasmids under the CAG-promoter. Results are representative of 4 independent experiments and quantifications are tabulated in Table S2. Scale bar, 100 μm.

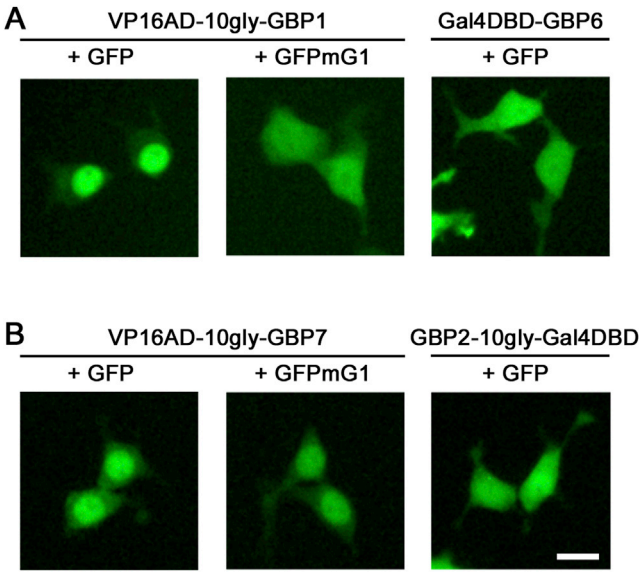

Figure S2. VP16AD-GBP Fusions Can Localize GFP to the Nucleus, Related to Figure 2

Representative images of GFP localization in 293T cells transfected with pCAG-GFP or pCAG-GFPmG1 along with CAG-driven DBDG or ADG plasmids at a 1:2 molar plasmid ratio. Fluorescent micrographs were taken at 16 hr post-transfection in live cells. Scale bar, 15μm.

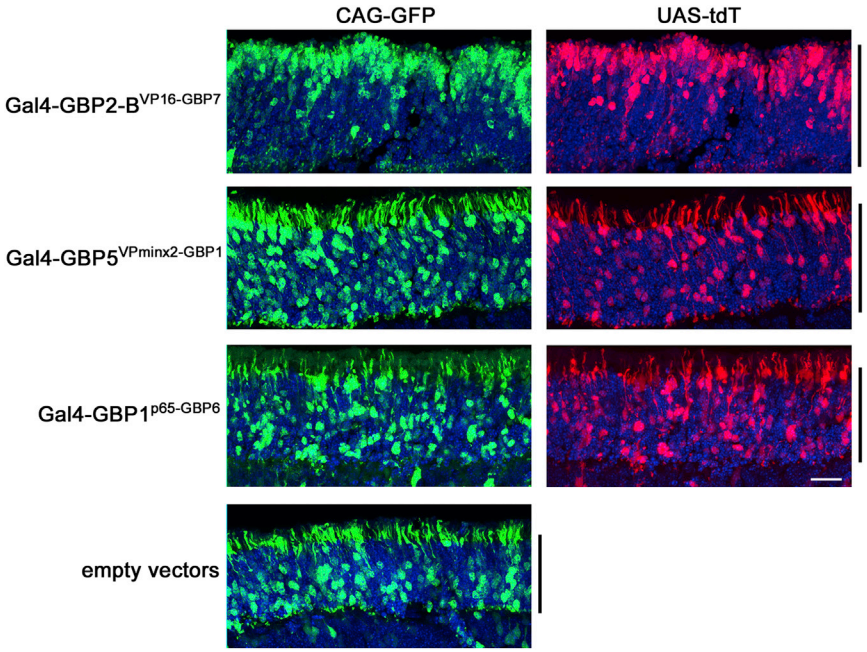

Figure S3. T-DDOGS Composed of VPminx2AD and p65AD Give Normal Positioning of Rod Photoreceptors in the Retina, Related to Figure 4
Representative images showing the effects of selected T-DDOGs on rod photoreceptor positioning. CD1 mouse retinas were electroporated at P0 in vivo with plasmids encoding CAG-GFP (green), Gal4-GBPX$^{AD-GBPY}$ components, UAS-tdT (red) and CAG-nlacZ. The electroporated GFP:DBDG:ADG plasmid mass ratio is 2:2:1. Retinas were harvested at P14. Confocal stacks of retina sections spanning the ONL (black bar) are shown. Each set of panels was adjusted individually to similar levels to reveal the cell bodies. DAPI is blue in all panels. Scale bar, 20 μm. Non-linear adjustment using the gamma function was applied to show weak GFP or tdT-expressing cells to minimize their signals from being obscured by those of stronger-expressing equivalents. The scleral portion of the ONL is the upper half of each image.

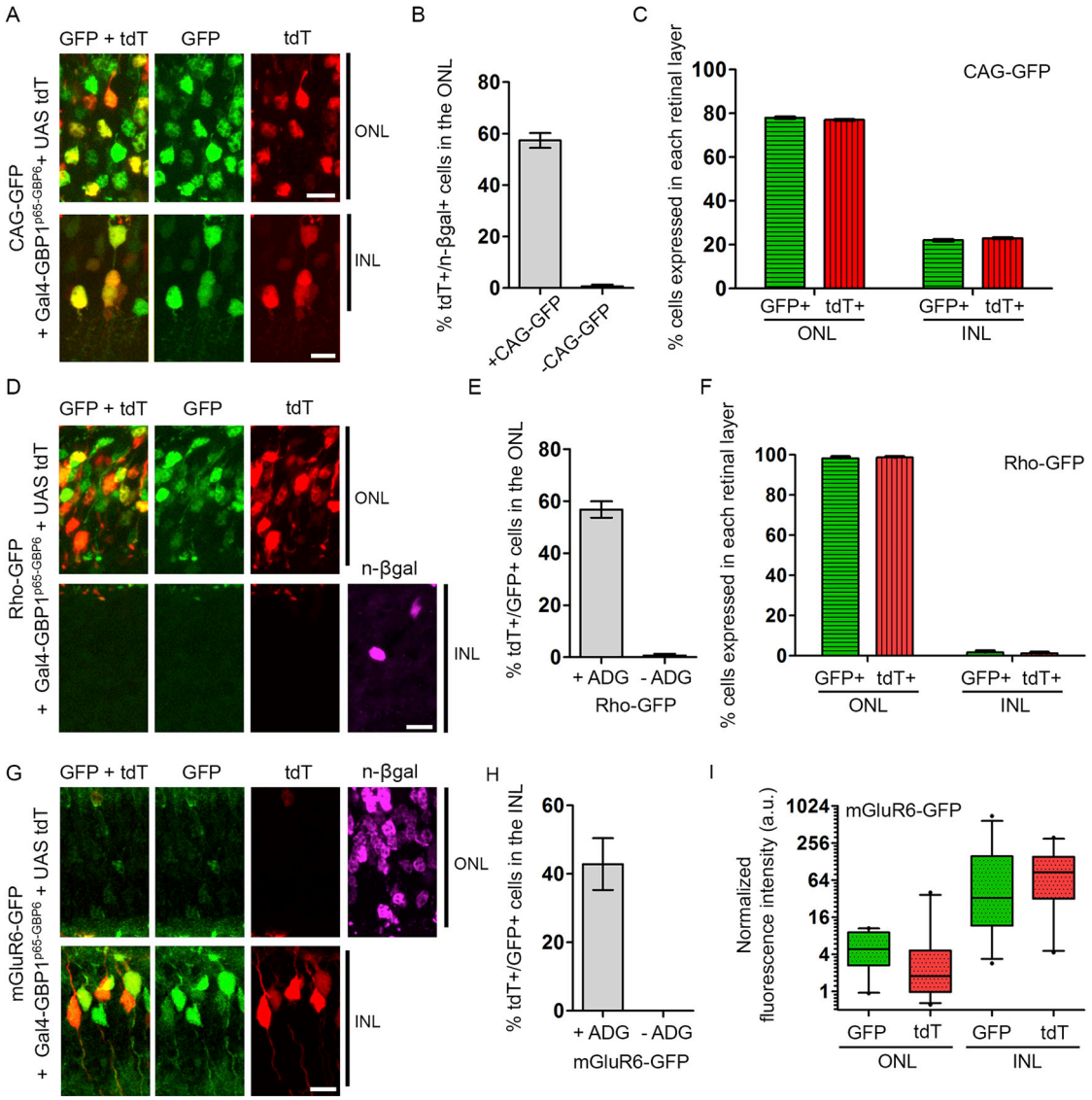

Figure S4. Quantification of Gal4-GBP1$^{p65\text{-}GBP6}$ Activities in the Retina, Related to Figure 4

Refer to Figure 4 and Experimental Procedures for experimental setup.

(A, D, and G) Colocalization of different promoter-driven GFP (green) with tdT (red) in retinas expressing Gal4-GBP1$^{p65\text{-}GBP6}$.

(B, E, and H) Efficiency and specificity of Gal4-GBP1$^{p65\text{-}GBP6}$ in vivo. Removal of CAG-GFP (B) or ADG (E, H) abolished reporter expression. In (B), the ordinate shows the percentage of tdT-expressing cells among the electroporated cells in the ONL, as assessed by expression of the electroporation marker, n-βgal. n-βgal detection and/or expression were poor in the INL, preventing analysis of Gal4-GBP1$^{p65\text{-}GBP6}$ efficiency in the INL from the sample in (B).

(C and F) Distribution of GFP and tdT expressing cells in electroporated retinas. Weak, leaky mGluR6-GFP expression in the ONL made it difficult to perform this analysis by cell-counting. (I) Quantification of fluorescent intensity of cells expressing GFP and tdT in (G). Boxplots indicate median, interquartile range, and 5%–95% range. *y* axis is on log2 scale. n = 25 each condition. For (B), (C), (E), (F), (H), plots are mean and SD. Scale bar, 10 μm. Note the tdT+/GFP+ data points for Rho-GFP, +ADG (E) and mGluR6-GFP, +ADG (H) were also presented in Figure S5 for a different argument.

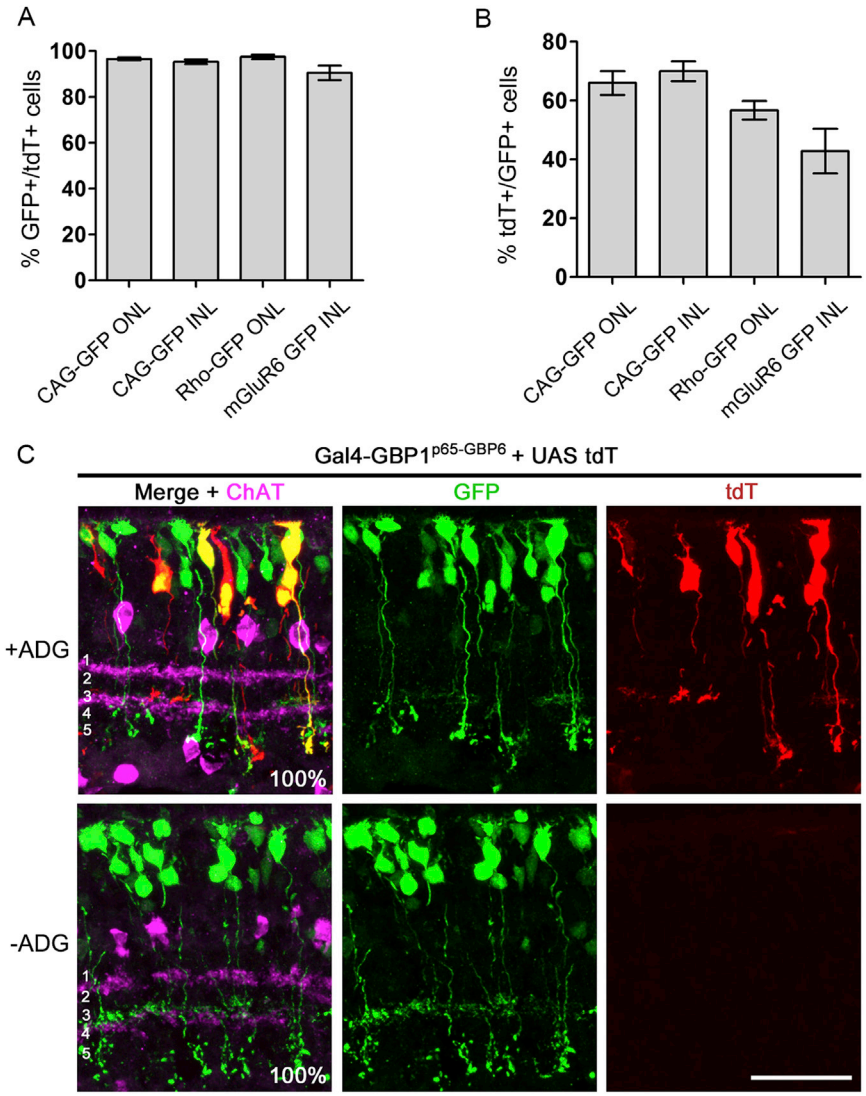

Figure S5. Additional Analysis of Electroporated Retinas from Figure S4, Related to Figure 4

Refer to Figure 4 and Methods for experimental setup.

(A) Tight-coupling of tdT+ cells with GFP expression. Among cells that expressed tdT, the percentage of cells expressing GFP is shown.

(B) Efficiency of tdT activation in GFP-expressing cells. Percentage of tdT+ cells among GFP+ cells. Note the tdT+/GFP+ data points for Rho-GFP and mGluR6-GFP were also presented in Figure S4 for a different argument. Plots show mean ± SD. See Table S3 for summary.

(C) mGluR6-GFP bipolar cells project to the correct IPL sublaminae in the presence of Gal4-GBP1$^{p65\text{-}GBP6}$. CD1 mouse retinas were electroporated at P0 with plasmids encoding mGluR6-GFP (green), Gal4-GBP1$^{p65\text{-}GBP6}$, UAS-tdT (red) and CAG-nlacZ. Retinas stained for anti-GFP (green) and anti-ChAT (magenta). The IPL is divided into 5 sublaminae (white font in merge panels), with the ON bipolar cells stratifying below the midline dividing sublaminae 2 and 3. Anti-ChAT labels the boundary between sublaminae 1 and 2, and also the boundary between 3 and 4. % GFP+ and GFP+/tdT+ cells stratifying below the midline of 2 and 3 are shown in merge panels. n = 28 for +ADG condition and n = 31 for –ADG condition. Cells were sampled across two retinas per condition. Scale bar, 20 μm.

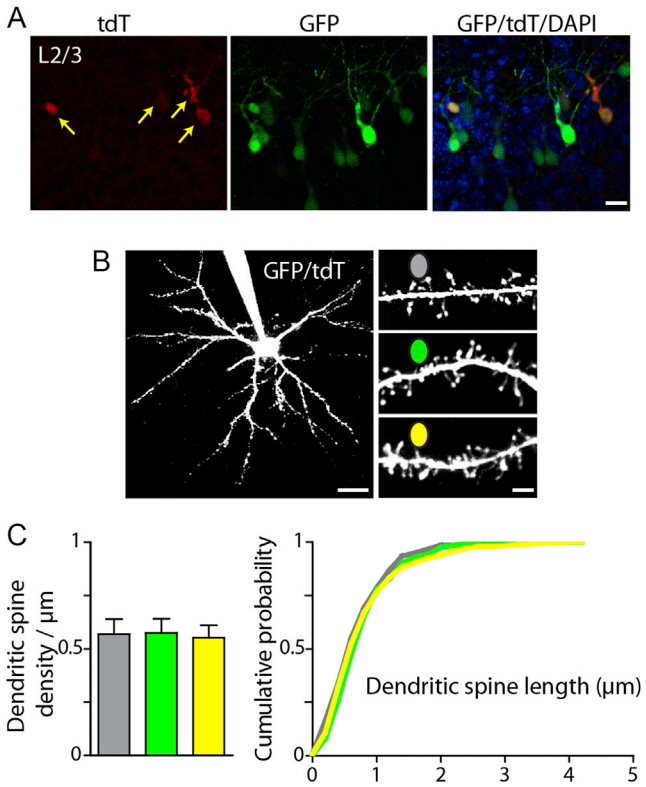

Figure S6. Structural Analysis of Electroporated Cortical Pyramidal Neurons, Related to Figure 5

Primary somatosensory cortex was electroporated at E15.5 with plasmids encoding GFP, ADG, DBDG, and UAS-tdT. T-DDOG is Gal4-GBP1$^{p65\text{-}GBP6}$.

(A) Confocal image of native GFP and tdT fluorescence in layers 2/3 of mouse primary somatosensory cortex. Red, tdT; green, GFP; overlay shows both channels with DAPI. A subset of GFP+ cells are tdT+, reflecting co-electroporation of 4 constructs. Arrows point to GFP+/tdT+ cells. Scale bar, 20 μm.

(B) Left, 2-photon Z-stack through a GFP+/tdT+ layer 2/3 pyramidal neuron filled with Alexa-594 through a patch pipette. Right, dendrites from GFP-, GFP+/tdT- and GFP+/tdT+ neurons at P13. Scale bars, 30 and 3 μm.

(C) Summary data of dendritic spine density (left) and length (right) for electroporated pyramidal neurons at P12-14. Dendritic spine density and length did not differ among GFP-, GFP+/tdT- and GFP+/tdT+ neurons. (Dendritic spine density, n = 7 neurons and 15-24 dendrites per condition; spine length, ~300 dendritic spines per condition). No GFP-/tdT+ neurons were observed in acute slices during recording or 2-photon imaging (n = 7 mice). Column plots are mean ± SEM.

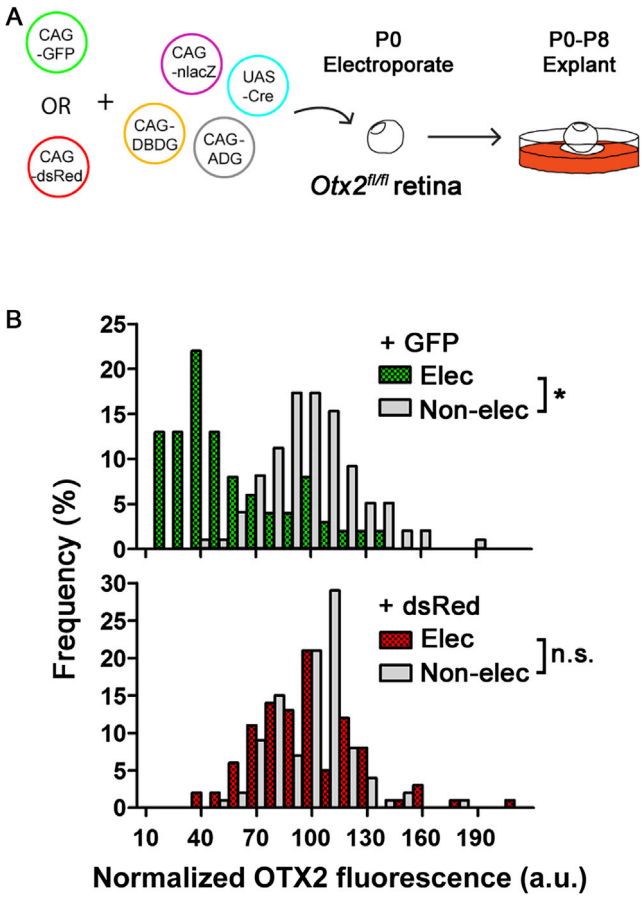

Figure S7. Excision of *Otx2*$^{fl/fl}$ Led to Decrease in OTX2 Protein Levels, Related to Figure 5

(A) Schematic of experiment. T-DDOG is Gal4-GBP1$^{p65\text{-}GBP6}$.

(B) OTX2 protein levels were measured by OTX2 immunofluorescence in single electroporated (Elec), GFP+ or dsRed+/n-βgal + cells in the ONL. Measured values are normalized against that of non-electroporated cells (Non-elec), judged by absence of GFP, dsRed and n-βgal. n = 100 each condition. * indicates $p < 0.0001$. n.s., not significant.